Master's Thesis

A TOA-DOA HYBRID FACTOR GRAPH-BASED TECHNIQUE FOR MULTI-TARGET GEOLOCATION AND TRACKING

1910113 Lei JIANG

Supervisor:	Tadashi Matsumoto
Main Examiner:	Tadashi Matsumoto
Examiners:	Brian M. Kurkoski
	Mineo Kaneko
	Tatsuhiro Nakada

School of Information Science
Japan Advanced Institute of Science and Technology

January 2021

I certify that I have prepared this Master's Thesis by myself without any inadmissible outside help.

Lei, JIANG
JAIST, 3 January 2021

Author: _____

Data: _____

Supervisor: _____

Abstract

In this thesis, we propose a new distributed sensors-based multi-target geolocation and tracking technique. The proposed technique is a joint time-of-arrival (TOA) and direction-of-arrival (DOA) factor graph (FG) for multi-target geolocation (FG-GE), which is further combined with another FG for extend Kalman filtering (FG-GE-EKF) for tracking. Two-dimensional (2D) and three-dimensional (3D) scenarios are considered. In the FG-GE part, a new sensor association technique is proposed to solve the matching problem, which makes the correct correspondence between the DOA/TOA information gathered by the distributed sensors and each target. With the proposed sensor association technique, the measured signals from targets can adequately be matched to their corresponding FGs. Thereby, the multi-target geolocation can be reduced to multiple independent single target geolocation. In addition, in the 3D scenario, each target is projected onto three orthogonal planes in the (x, y, z) coordinate. With the projection, the 3D geolocation is decomposed into three 2D geolocation problems. In the FG-GE-EKF part, the whole tracking system can be divided into two steps: prediction step and update step. In the prediction step, the predicted state is obtained from the previous state. Then, we utilize the predicted state as *a* prior information, and also to update the message exchanged in FG-GE. In the update step, the estimates obtained by FG-GE are regarded as observation state which is used to refine the predicted state, and to acquire the current state. With proposed the FG-GE-EKF, the position estimation accuracy and tracking performance can be improved dramatically, without requiring excessively high computational effort.

Keywords: Factor graph (FG), time of arrival (TOA), direction of arrival (DOA), geolocation, extend Kalman filter (EKF), tracking, sensor association.

Acknowledgment

First of all, I would like to express my sincere gratitude to my supervisor Prof. Tadashi Matsumoto, who gave me a chance to pursue a Master degree in Japan. During the passed two years, he has offered me valuable suggestions in academic study. Without his patient guidance, this thesis would not been completed.

Besides, I am grateful to all the lab members. Thanks to Prof. Brain M. Kurkoski for his suggestions and help. Thanks to Dr. Meng Cheng, who helps me a lot not only on the research work but also in daily life. Thanks to the lab members Shulin Song, Wu Li, Ning Liu for sharing the happiness.

Finally, I would like to thanks to my parents. They always give me a lot of support and encouragement.

List of Abbreviations

2D	Two-dimension
3D	Three-dimension
5G	Fifth generation
B5G	Beyond fifth generation
CEO	Chief executive officer
CRLB	Cramér–Rao lower bound
DHT	Distributed hypothesis testing
DOA	Direction of arrival
DOA-FG	Direction-of-arrival based factor graph
EKF	Extend Kalman filter
FG	Factor graph
FG-GE	FG-based geolocation
FG-GE-EKF	FG based geolocation and EKF tracking
GNSS	Global Navigation Satellite System
GPS	Global Positioning System
IoT	Internet of Things
KF	Kalman filtering
LBS	Location-based services
MAP	Maximum a posteriors probability
MIMO	Multiple-input multiple-output
ML	Machine leraning
mmWave	Millimeter-wave
RMSE	Root Mean Square Error
RSS	Received-signal-strength
SPA	Sum-product algorithm
SSM	State-space models
TDOA	Time-difference-of-arrival
TDOA-FG	Time-difference-of-arrival based factor graph
TOA	Time of arrival
TOA-FG	Time-of-arrival based factor graph
TS	Taylor series

List of Symbols

$(\cdot)^{-1}$	Matrix inverse operation
$(\cdot)^{T}$	Transpose of matrix
$(\cdot)_{\rightarrow}$	The direction of message flow over the FG
β	Central point for $1^{st}TS$
λ_i	Constants of DOA approximation
τ_i	Constants of TOA approximation
$\frac{\partial \varphi}{\partial x}$	The first derivation of φ over x
$F(s)$	Fisher information matrix
$g(\cdot)$	Global function
$f_A(\cdot)$	Local function at factor node A
J	Jacobin matrix
k	Time index
$m_{(\cdot)}$	Mean of the message
$\sigma^2_{(\cdot)}$	Variance of the message
$u_{n,k}$	Measurement error of DOA
$v_{n,k}$	Measurement error of TOA
$p(\cdot)$	Probability density function
υ	Angle between sensor and projected point on the plane (x, z)
γ	Angle between sensor and projected point on the plane (y, z)
(X_n, Y_n)	Sensor position with n-th sensor in 2D
(X_n, Y_n, Z_n)	Sensor position with n-th sensor in 3D
c	Speed of light
$\mathbf{e}_k$	Observation noise at timing k
$\mathbf{j}_k$	Observation state at timing k
$\mathbf{s}_{k\|k-1}$	Predicted state of target position
$\mathbf{s}_k$	Current state of target position at timing k
$\mathbf{v}_{k\|k-1}$	Predicted velocity at timing k
$\mathbf{v}_k$	Velocity at timing k
$\mathbf{w}_k$	Current white Gaussian noise of SSM at timing k
$\sum_{\sim x_i}$	The summary operator for x_1
(x_i, y_i)	target position with i-th target in 2D
(x_i, y_i, z_i)	target position with i-th target in 3D
$(\hat{x}_i, \hat{y}_i, \hat{z}_i)$	target position estimate with i-th target in 3D
$(\hat{x}_i, \hat{y}_i)$	target position estimate with i-th target in 2D

$\triangle t$	Time difference between target and sensor
$\hat{d}_{2D,n,k}$	Measured TOA with n-th sensor at timing k in 2D
$\hat{d}_{3D,n,k}$	Measured TOA with n-th sensor at timing k in 3D
$h(\cdot)$	True DOA
$q(\cdot)$	True TOA
$\hat{\theta}_{n,k}$	Measured elevation DOA with n-th sensor at timing k
$\hat{\varphi}_{n,k}$	Measured azimuth DOA with n-th sensor at timing k

List of Figures

List of Tables

Contents

Chapter 1

Introduction

1.1 Background and Motivation

Wireless geolocation, also known as localization or position detection, is a technology that uses distributed sensors to accurately identify the location of radio emitters [3]. By obtaining measurements such as the propagation angle, time and intensity of electromagnetic waves, the geolocation systems aim to estimate radio emitter's positions in the spatial coordinate.

In future wireless communication networks, wireless geolocation technology is an indispensable link to every corner of the society, especially in the smart city, smart vehicular communications systems, intelligent navigation and other applications [4–6]. The demand for location-based services (LBS) and applications have become more diversified with the rapid development of technology, especially in today's booming Internet of Things (IoT) business: in terms of indoor location services, it provides users with indoor navigation, indoor car search and location social services [7]; in public safety and emergency rescue, such as Enhanced-911 [4], firefighters and policemen can quickly start a rescue operation by accurately locating the victims; in factories, managers want to keep track of precious materials and production equipment accurately [8]; in driving, the driver wants to find the smoothest route and the nearest parking space [9, 10]; the realization of smart home is inseparable from the accurate positioning of users [11, 12], as in Fig. 1.1. Moreover, when the fifth generation (5G) and beyond fifth generation (B5G) mobile wireless communication systems are considered, accurate geolocation techniques for position-related services are required. For example, when beamforming [13–15] is applied in 5G systems to eliminate the effects of detrimental attenuation in millimeter-wave (mmWave) signaling, target tracking in massive multiple-input multiple-output (MIMO) systems is of significant importance to ensure the effectiveness of beamforming, as shown in Fig. 1.2.

It should be noted that Global Positioning System (GPS) and Global Navigation Satellite System (GNSS) provide users with location service [16],

Figure 1.1: Wireless geolocation in various applications

which basically solves the problem of accurate positioning in outdoor space and has been widely used in daily life. However, in the indoor environment, GNSS positioning accuracy is significantly degraded due to the influence of building shielding and multi-path effects, which cannot meet the accuracy requirements of indoor location services. Besides, when stand-alone radars are considered, they usually require large scale hardware. Therefore, in this research, distributed sensors instead of stand-alone radars are used to detect and track the position of the target. This is because (1) compared to such stand-alone radar systems, the distributed sensors are more flexible to be located without requiring high hardware cost; (2) the distributed sensors can be installed in both indoor and outdoor environments quickly, and the high accuracy can be expected for wireless geolocation.

In wireless geolocation algorithm, the mathematical framework is, in common, nonlinear, and the direct calculation of the multi-target positions, including combinatory problems, is highly complex. To solve the problems, a framework using factor graph (FG) has been proposed [1]. FG-based geolocation (FG-GE) techniques do not require high computational complexity due to the fact that only means and variances of the messages derived from the measurements, which is assumed to suffer from Gaussian-distributed measurement error, is exchanged between the nodes in the FG [17]. To keep the Gaussianity of the messages exchanged in FG, the first order Taylor series (TS) expansion is applied to approximate the trigonometric functions by linear functions [18].

In practical application, compared with static target positioning, dynamic

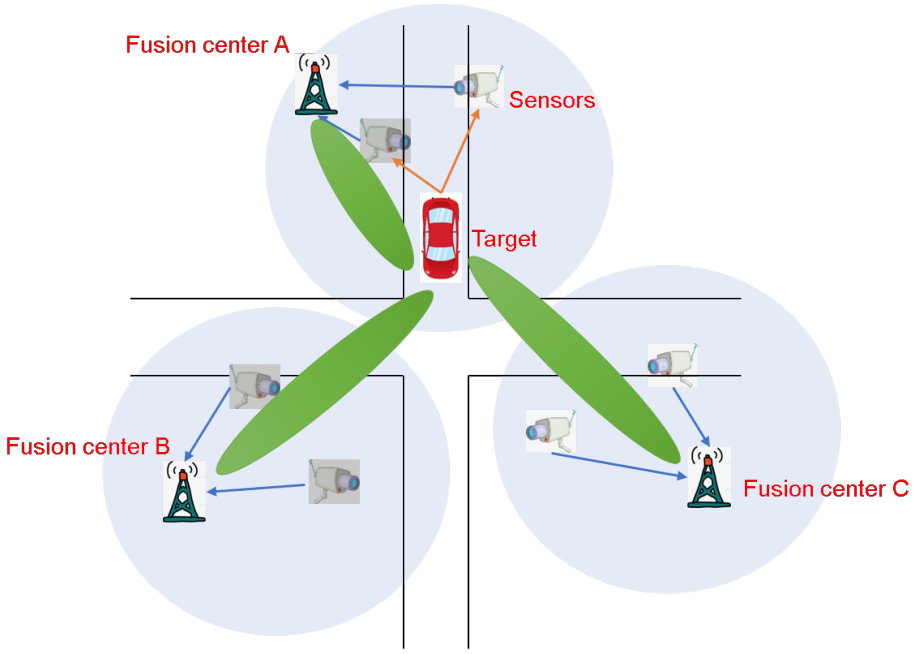

Figure 1.2: Beamforming based on wireless geolocation

target tracking is more widely used, leading to more complex problems. Nowadays, target tracking technology is always accompanied by geolocation technologies, which also plays an important role in many fields, such as robot motion tracking, trajectory correction of the rocket, autopilot systems and eyeball-tracking technique [19–22]. Therefore, in addition to multi-target target geolocation, another purpose of this research is to achieve dynamic multi-target tracking.

The background described above has motivated this research. In this thesis, a new joint time of arrival (TOA) - direction of arrival (DOA) technique is proposed not only to compensate each technique's shortcomings but also to solve the problem of associated to the observation and target positions. The combined FGs for geolocation and extend Kalman filter (EKF) can be used not only to estimate the positions of the static multiple targets, but also to track their trajectories dynamically.

1.2 Related Work

In recent years, in-depth discussions on a variety of indoor geolocation services and their evolution scenarios [23] have been taking place in industry. [24] presents a technique that localizs multiple persons by utilizing on the

reflections of wireless signals reflected from their bodies. However, calculation for the intersection of several ellipses needs high computational effort because of their non-linear properties. A multi-target localization technique based on machine leraning (ML) is introduced in [25]. In general, extensive prior training is required in the ML algorithms including recording of each position feature. Also, database construction is needed to store the data.

In this research, comapred with other localization techniques, we only focus on the FG-based geolocation technique due to the fact that the proposed FG algorithm requires lower computational complexity because (1): it decomposes the complex global function with many variables into a product of several local functions with a few variables; (2): The message passing process performed in the factor graph requires only means and variances, owing to the Gaussian distribution of the measurement error. Nevertheless, after several iterations, the FG-based message passing algorithm can achieve maximum a posteriors probability (MAP) estimates of the target positions by using the sum-product algorithm for the probability marginalization.

In the conventional FG based geolocation systems, different types of wireless parameters such as DOA [26], TOA [27], time-difference-of-arrival (TDOA) [28] and received-signal-strength (RSS) [29,30] are used. The time-difference-of-arrival based factor graph (TDOA-FG), time-of-arrival based factor graph (TOA-FG), direction-of-arrival based factor graph (DOA-FG) have been proven to be useful for the detection of single target position. However, FG-based accurate position identification of multiple anonymous[1] targets has not yet been matured. When multiple targets have the same distance to some of the distributed sensors, it is difficult to accurately identify multiple target positions with the TOA/TDOA because the time of arrival of the waves at those sensors are almost the same, which indicates the time difference of arrival is almost zero. On the other hand, when multiple targets are located on the same line originating from the some of the sensors, or when the angle difference is small, the DOA detection is unreliable. For the RSS-based technique, off-line training using reference signals from monitoring spots is required beforehand, which can not be obtained from multiple anonymous targets case.

In the conventional tracking systems, different types of tracking algorithm have been proposed. The concept of Lucas-Kanade algorithm was first proposed by [31]. By using the pixel relation between adjacent frames of video sequence, the motion state of the target can be judged by looking for the displacement change of the pixel, so as to realize the tracking of

[1]The terminology "anonymous" is defined as the unknown device emitting radio wave where the sensors/receives have no any knowledge about the emitter [3].

the moving target. However, the poor real-time performance cannot be avoided by computing all the pixels in the video. Kalman filtering (KF) is an algorithm that can effectively predict the location of the target [32]. It utilizes the knowledge of the dynamics of the target behavior, expressed by state-space equation, utilizes the observed data in the state-space equation, and achieves the most likely estimates. KF algorithm is only applicable to linear Gaussian Markov model. [33] proposes a technique successfully utilizing deep learning technique for target tracking. The tracking technique based on deep learning requires a high resolution of the images on the data set, otherwise, the training classifier cannot obtain effective features and has poor tracking performance.

Therefore, in this research, to achieve high multi-target tracking accuracy in dynamic scenarios, the EKF technique is used to solve the problems as described above. The target positions estimated by FG-GE can be regarded as observation state in the tracking process. However, the variance of the observation error can not be directly detected. Instead, the smallest variance of the observation which can be determined by the Cramér–Rao lower bound (CRLB) is used as the variance of the observation error. The proposed algorithm that combines FGs for GE and EKF is referred to as FG based geolocation and EKF tracking (FG-GE-EKF) for the notation convenience commonly in this thesis.

1.3 Research Contribution

This research focuses on distributed sensors-based geolocation technique. The main contributions of this research are summarized as follows.

1. First of all, a new two-dimension (2D) joint TOA-DOA based FG is proposed for multi-target geolocation and tracking by integrating the EKF algorithm into a unified FG. Furthermore, the proposed technique is then extended to a three-dimension (3D) scenario.
2. A new sensor association algorithm based on the joint TOA-DOA measurements is proposed to solve the target-observation matching problem occurring typically in the distributed sensors systems, both in 2D and 3D scenarios.
3. A switching algorithm for the use of either TOA or DOA is proposed to alleviate the shortcomings inherent in TOA-only and DOA-only algorithms as described before.

1.4 Thesis Outline

The structure of this thesis is illustrated as in Fig. 1.3, and organized as follows:

In Chapter 1, the background, motivation and related work of this research have been already described. We have also summarized the contributions and provided the outline of this research.

In Chapter 2, the overview of factor graph and sum-product algorithm is discussed. Also, the fundamental concepts of TOA, DOA and EKF are described.

In Chapter 3, we present the proposed FG-based joint TOA-DOA techniques for multi-target geolocation in the 2D and 3D scenarios.

In Chapter 4, the FG-based EKF algorithm is detailed, and performance evaluation results by simulations are presented.

In Chapter 5, information theoretic background and relationship between chief executive officer (CEO) and distributed hypothesis testing (DHT) problems from the viewpoint of geolocation is briefly provided.

In Chapter 6, we conclude the thesis with some concluding remarks and future work.

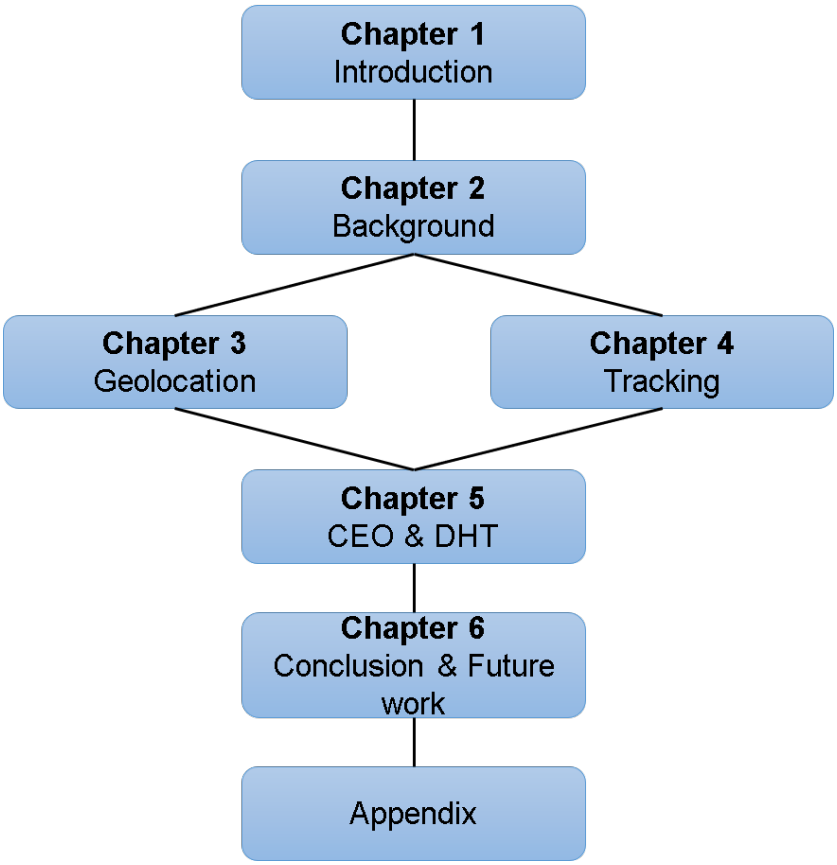

Figure 1.3: The structure of the thesis

Chapter 2

Research Background

In this chapter, we provide the background of the techniques used in the thesis. First of all, the overview of factor graph (FG) and sum-product algorithm (SPA) are introduced. Then we provide the fundamental concepts of geolocation and Kalman filter (KF) using the FG.

2.1 Overview of Factor Graph and Sum-Product Algorithm

Factor graph (FG) is a technique to graphically factorize the global function into several local functions [2]. The sum-product algorithm (SPA) is an efficient technique to calculate marginal probability of the global function, and to finally obtain the maximum a posteriors probability (MAP) estimates. In this thesis, we use the terminology "message passing" instead of the "sum-product algorithm", because "message passing" includes broader concept and the fact that we use the sum-product algorithm can easily be understood from the messages and FG expressions.

As in [1], an example of FG, which consists of factor nodes and variables nodes, represented as square and circle, respectively, is shown in Fig. 2.1. Let $g(x_1, x_2, x_3, x_4, x_5)$ be a global function with five variables, Assume that it is expressed as a product of several local functions, as

$$g(x_1, x_2, x_3, x_4, x_5) = f_A(x_1) f_B(x_2) f_C(x_1, x_2, x_3) f_D(x_3, x_4) f_E(x_3, x_5), \quad (2.1)$$

where $f_H(\cdot)$, $H \in \{A, B, C, D, E\}$ denotes the local functions. Use x_3 as an example, the marginal function of x_3 can be computed as

$$
\begin{aligned}
g(x_3) &= \sum_{\sim\{x_3\}} g(x_1, x_2, x_3, x_4, x_5) \\
&= \left(\sum_{\sim\{x_3\}} f_A(x_1) f_B(x_2) f_C(x_1, x_2, x_3) \right) \\
&\times \left(\sum_{\sim\{x_3\}} f_D(x_3, x_4) \right) \times \left(\sum_{\sim\{x_3\}} f_E(x_3, x_5) \right),
\end{aligned} \tag{2.2}
$$

where $\sim \{x_3\}$ refers to all the variables except x_3. As in Fig. 2.2, the messages exchanged between the factor nodes and the variable nodes can be defined as follow [1]:

- Variable to local function

  The message passing from the variable node x to the local function factor node f, denoted by $\mu_{x\to f}(x)$, can be computed by the product of messages from neighbors as

$$
\mu_{x\to f}(x) = \prod_{h\in n(x)\setminus\{f\}} \mu_{h\to x}(x) \tag{2.3}
$$

- local function to variable

  The message passing from the local function factor node f to the variable node x, denoted by $u_{f\to x}(x)$, is the product of the local function with all the messages coming from variables except the destination variable, which can be expressed as

$$
u_{f\to x}(x) = \sum_{\sim\{x\}} \left(f(X) \prod_{y\in n(f)\setminus\{x\}} u_{y\to f}(y) \right), \tag{2.4}
$$

  where $X = n(f)$ denotes the local function f.

In this thesis, we are interested in computing the several marginal functions related to the estimates of target position in the (x, y) or (x, y, z) coordinate. The details of the proposed techniques will be discussed in Chapter 3 and 4.

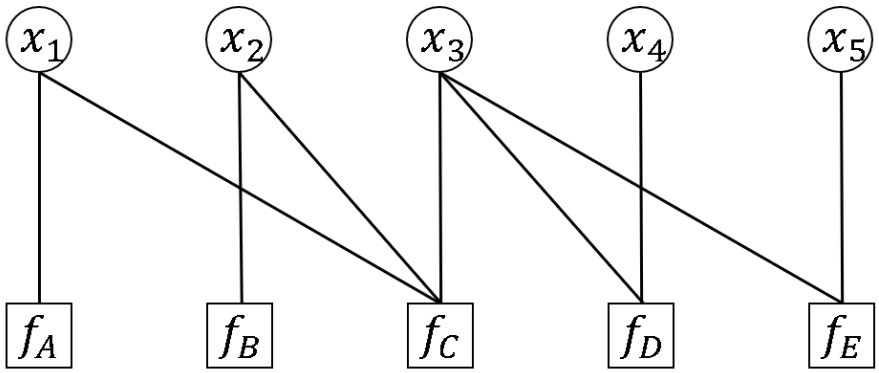

Figure 2.1: The example of a simple factor graph

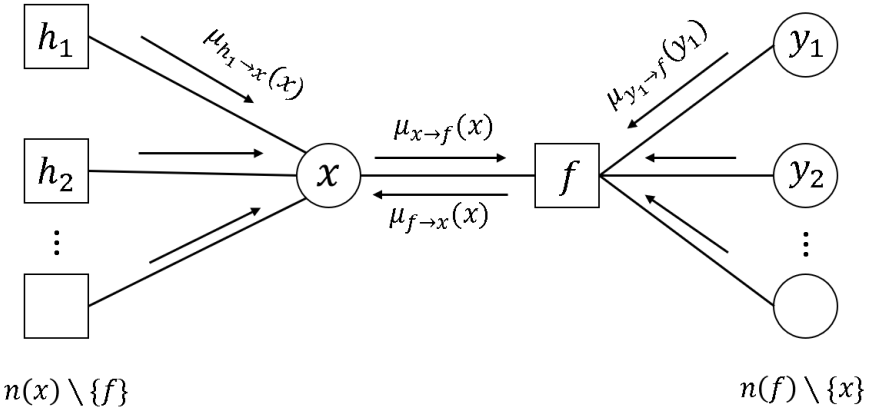

Figure 2.2: Message exchanges between factor nodes and variable nodes [1]

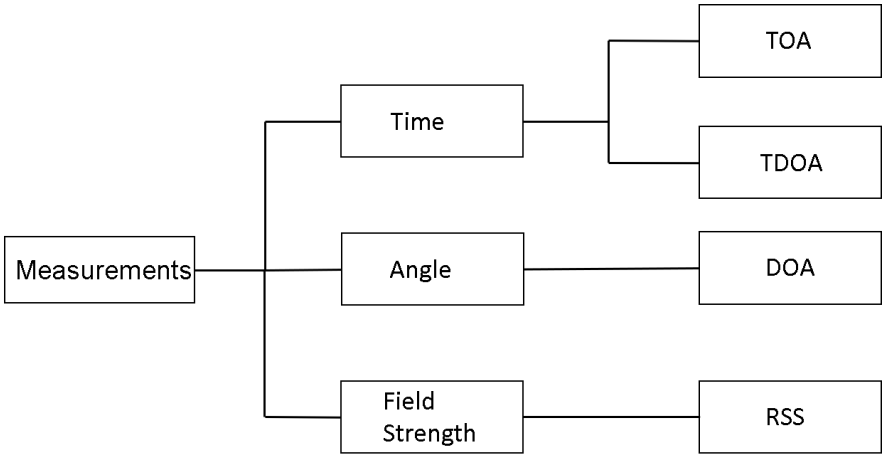

Figure 2.3: Geolocation category with different measurements

2.2 Overview of Geolocation

Accurate wireless geolocation has been expected to play crucial roles for position-related services and applications. Wireless geolocation refers to the operations for estimating the position of the target from the measurements of various wireless parameters using the specific algorithms. The received measurements information mainly includes three categories: time category, angle category, electromagnetic field strength category. The geolocation techniques and algorithms are different according to the categories of the measurements, as shown in Fig. 2.3. Each technique has its own advantages and disadvantages, as described before. In this research, we focus on the joint TOA-DOA geolocation technique, because we consider that their inherent shortcomings can easily be compensated.

2.2.1 TOA-based Measurement

Time of arrival (TOA) measurement indicates measuring the time difference between the signal departure t_0 from the target and arrival t_i at sensor i. The time difference $\triangle t = t_i - t_0$. The measurement of TOA can be converted to the Euclidean distance between the target and the sensors by

$$d_i = \triangle t \cdot c, \tag{2.5}$$

where $c = 3 \times 10^8$ meter/second is the light speed. The position of the target can then be obtained from the TOA measurement as

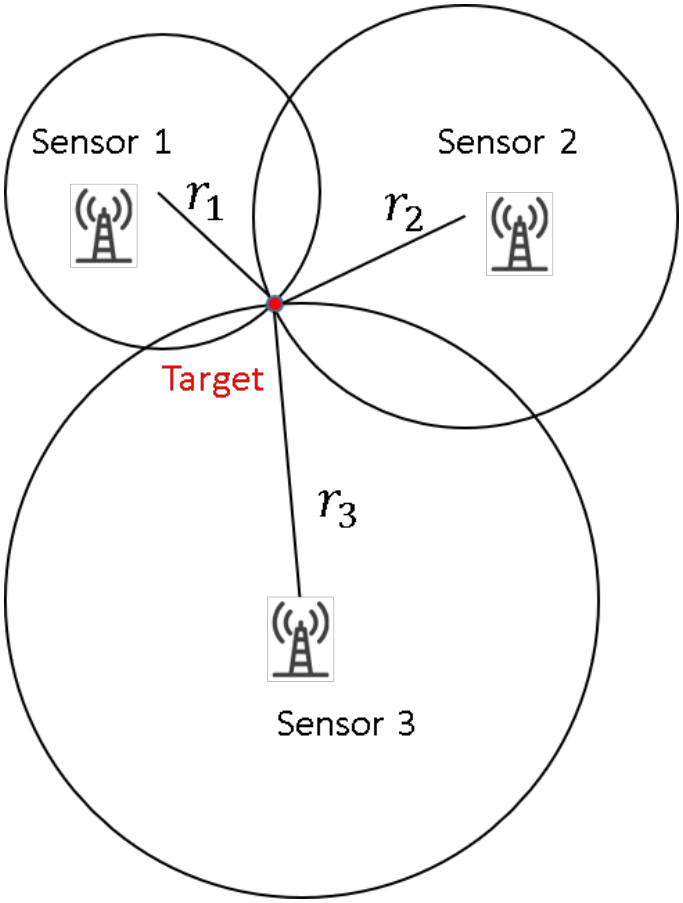

Figure 2.4: Geolocation using TOA measurement

$$\hat{d}_i = \sqrt{(X_i - x)^2 + (Y_i - y)^2}, \tag{2.6}$$

where (X_i, Y_i) and (x, y) are the positions of sensor i and target, respectively. At least three distributed sensors are needed to estimate the position of the target, as shown in Fig. 2.4

The Euclidean distances between the distributed sensors and the target are r_1, r_2 and r_3, respectively, in Fig. 2.4. Three circles can be obtained by using the position of each sensor as the centre. Then the Euclidean distances corresponds to the radius. The intersection point of three circles is the position of target.

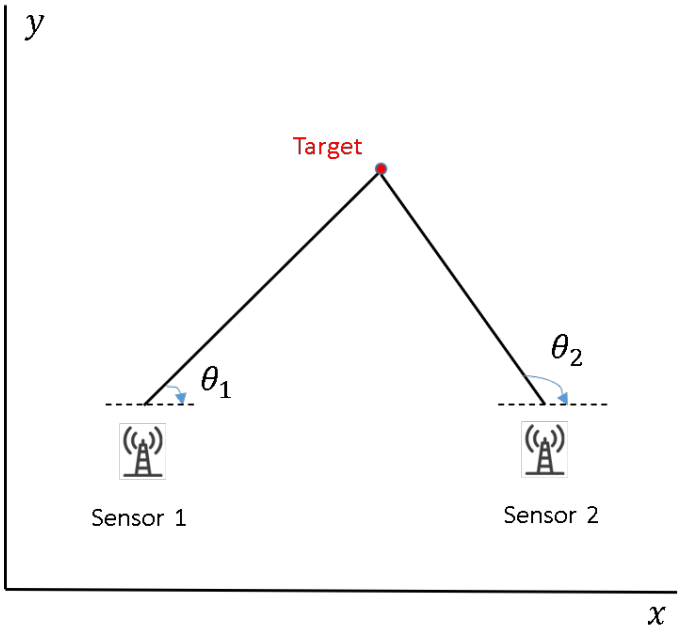

Figure 2.5: Geolocation using DOA measurement

2.2.2 DOA-based Measurement

Direction of arrival (DOA) measurement indicates the direction information of the coming signal from the target. DOA geolocation technique focuses on estimating the position of the target by using the angle measurement θ_i between the target and sensor i. The model of DOA can be given by

$$\hat{\theta}_i = \arctan\left(\frac{Y_i - y}{X_i - x}\right), \tag{2.7}$$

where (X_i, Y_i) and (x, y) are the positions of sensor i and target, respectively. By using DOA geolocation technique, only two distributed sensors are required, as shown in Fig. 2.5. Using the positions of two distributed sensors as the originating point, two lines are formed from the each originating points. The position of the target is the intersection points of the two lines. It should be noted that DOA-based FG geolocation techniques need at least three sensors, as described in Chapter 3.

2.3 Overview of Tracking

2.3.1 Kalman filter

Kalman filter (KF) is an efficient recursive estimation technique, which can be used to estimate the state of dynamic systems from a series of measurements suffering from measurement error. It has been proven to be useful in a wide variety of applications, such as vehicle tracking, navigation systems, stock prediction, and etc.

In general, the Gaussian-Markov state-space models (SSM) are used for the tracking. As in [2], the system SSM can be defined as

$$\mathbf{x}_k = \mathbf{A}_k \mathbf{x}_{k-1} + \mathbf{B}_k \mathbf{v}_k, \tag{2.8}$$

$$\mathbf{y}_k = \mathbf{C}_k \mathbf{x}_k + \mathbf{D}_k \mathbf{w}_k, \tag{2.9}$$

where $k = \{1, 2, \cdots, N\}$ is the time index, $\mathbf{v}_k$ and $\mathbf{w}_k$ are independent zero-mean Gaussian noise with $\mathbf{v}_k \sim \mathcal{N}_{\mathbf{v}_k}(0, \mathbf{I}_K)$ and $\mathbf{w}_k \sim \mathcal{N}_{\mathbf{w}_k}(0, \mathbf{I}_M)$. In this research, we assume time-invariant SSM, and hence the time index k is eliminated from $\{\mathbf{A}_k, \mathbf{B}_k, \mathbf{C}_k, \mathbf{D}_k\}$. We focus on factor graph (FG) and the sum-product algorithm (SPA) based tracking by using KF. The FG of KF can be illustrated in Fig. 2.6. It should be noted that all the messages passing over the FG are Gaussian distributed. Hence, only the means and the covariance matrix are exchanged over the FG for the messages processing at the nodes. The previous state and the predicted state can be denoted as

$$\mu_{f_{k-1} \to \mathbf{x}_{k-1}}(\mathbf{x}_{k-1}) = \mathcal{N}_{\mathbf{x}_{k-1}}(\mathbf{m}_{k-1|k-1}, \mathbf{P}_{k-1|k-1}), \tag{2.10}$$

$$\mu_{\mathbf{x}_k^{(1)} \to =}(\mathbf{X}_k^{(1)}) = \mathcal{N}_{\mathbf{X}_k^{(1)}}(\mathbf{m}_{k|k-1}, \mathbf{P}_{k|k-1}), \tag{2.11}$$

where $\mathbf{m}$ and $\mathbf{P}$ are the mean and covariance matrix, respectively. It should be noted that the incoming message to node f_k is $\mu_{f_{k-1} \to \mathbf{x}_{k-1}}(\mathbf{x}_{k-1})$, also known as the previous state at timing $k-1$. The outgoing message from node f_k is $\mu_{f_k \to \mathbf{x}_k}(\mathbf{x}_k)$, also known as the current state at timing k. The whole tracking process can be divided into two steps: prediction step and update step.

- Prediction step

$$\mathbf{m}_{k|k-1} = \mathbf{A}\mathbf{m}_{k-1|k-1}, \tag{2.12}$$

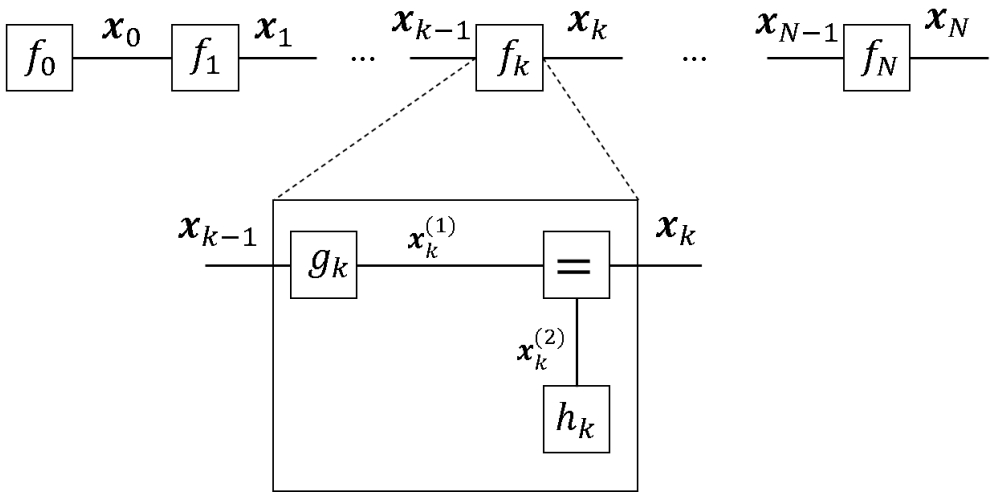

Figure 2.6: the structure of KF based on FG [2]

$$\mathbf{P}_{k|k-1} = \mathbf{A}\mathbf{P}_{k-1|k-1}\mathbf{A}^T + \mathbf{B}\mathbf{B}^T. \tag{2.13}$$

- Update step

$$\mathbf{m}_{k|k} = \mathbf{m}_{k|k-1} + \mathbf{K}_k(\mathbf{y}_k - \mathbf{C}\mathbf{m}_{k|k-1}), \tag{2.14}$$

$$\mathbf{P}_{k|k} = (\mathbf{I} - \mathbf{K}_k\mathbf{C})\mathbf{P}_{k|k-1}, \tag{2.15}$$

where $\mathbf{K}_k = \mathbf{P}_{k|k-1}\mathbf{C}^T(\mathbf{D}\mathbf{D}^T + \mathbf{C}\mathbf{P}_{k|k-1}\mathbf{C}^T)^{-1}$.

2.3.2 Extend Kalman filter

KF can only be used on the premise that the variables are all Gaussian distributed. However, since our measurements and system models are nonlinear, conventional KF algorithm can not be utilized. Therefore, EKF is proposed to approximate the nonlinear system model by a linear function. The nonlinear system model can be given by

$$\mathbf{x}_k = f(\mathbf{x}_{k-1}) + \mathbf{w}_k, \tag{2.16}$$

$$\mathbf{y}_k = h(\mathbf{x}_k) + \mathbf{v}_k, \tag{2.17}$$

where $f(\cdot)$ and $h(\cdot)$ are nonlinear functions, $\mathbf{w}_k$ and $\mathbf{v}_k$ are zero-mean Gaussian distributed with $\mathbf{w}_k \sim \mathcal{N}(0, \mathbf{Q})$ and $\mathbf{v}_k \sim \mathcal{N}(0, \mathbf{R})$. In the same way as KF process, the EKF process can also be divided into two steps: the prediction step and the update step.

- Prediction step

$$\mathbf{x}_{k|k-1} = f(\mathbf{x}_{k-1|k-1}), \tag{2.18}$$

$$\mathbf{P}_{k|k-1} = \mathbf{F}_{k-1}\mathbf{P}_{k-1|k-1}\mathbf{F}_{k-1}^T + \mathbf{Q}_{k-1}. \tag{2.19}$$

  where matrix $\mathbf{F}$ is the Jacobian matrix of the function $f(\cdot)$.
- Update step

$$\mathbf{x}_{k|k} = \mathbf{x}_{k|k-1} + \mathbf{K}_k(\mathbf{y}_k - h(\mathbf{x}_{k|k})), \tag{2.20}$$

$$\mathbf{P}_{k|k} = (\mathbf{I} - \mathbf{K}_k\mathbf{H}_k)\mathbf{P}_{k|k-1}, \tag{2.21}$$

  where matrix $\mathbf{H}_k$ is the Jacobian matrix of the function $h(\cdot)$ and $\mathbf{K}_k = \mathbf{P}_{k|k-1}\mathbf{H}_k^T(\mathbf{H}_k\mathbf{P}_{k|k-1}\mathbf{H}_k^T + R)^{-1}$, however, again we assume time-invariant dynamics of the target behavior, we omit the time index k from $\mathbf{F}_k$ and $\mathbf{H}_k$, as $\mathbf{F}$ and $\mathbf{H}$.

Chapter 3

Factor Graph-based Geolocation

In this chapter, we focus on multi-target geolocation based on factor graph by using joint DOA-TOA measurements. The two-dimensional and three-dimensional scenarios are considered. The proposed system model and algorithms are detailed in the sub-chapter. The simulation results are also included in this chapter, which are used to evaluate the performance of the proposed algorithms.

3.1 Multi-target Position Detection in 2D scenario

3.1.1 System Model

We start with a 2D scenario system model. A joint time-of-arrival and direction-of-arrival measurements are used to estimate the multi-target positions. In the proposed technique, N distributed sensors locate at (X_n, Y_n), $n = \{1, 2, \cdots, N\}$, in the global coordinate. The position information of all the sensors are assumed to be known to the fusion center. I anonymous multiple targets are assumed to be located at $(x_{i,k}, y_{i,k})$, where $i = \{1, 2, \cdots, I\}$ and $k = \{1, 2, \cdots, K\}$ are the target and timing indexes, respectively.

For simplicity, the target index i is omitted unless required. The measurement of DOA at timing k can be given by

$$\hat{\varphi}_{n,k} = h(\varphi_{n,k}) + u_{\varphi,n,k} \tag{3.1}$$

with the measurement error $u_{\varphi,n,k} \sim \mathcal{N}(0, \sigma_{\varphi}^2)$, and $h(\varphi_{n,k})$ denotes the true DOA $\varphi_{n,k}$, which is given by

$$h(\varphi_{n,k}) = \arctan\left(\frac{Y_n - y_k}{X_n - x_k}\right). \tag{3.2}$$

The measurement of TOA at timing k is converted to Euclidean distance by

$$\hat{d}_{2D,n,k} = c \cdot \triangle t = q(d_{2D,n,k}) + v_{2D,n,k} \tag{3.3}$$

with the measurement error $v_{2D,n,k} \sim \mathcal{N}(0, \sigma_d^2)$, c the light speed and $\triangle t$ the time difference between the transmit and receive timings. $q(d_{2D,n,k})$ denotes the true TOA, which is given by

$$q(d_{2D,n,k}) = \sqrt{(X_n - x_k)^2 + (Y_n - y_k)^2}. \tag{3.4}$$

In this thesis, we assume that the sensors and targets share the same time reference, such as in aviation control or commercial navigation systems.

3.1.2 Sensor Association

In this thesis, all of the targets are anonymous. Thus, the matching problem between distributed sensors' observations and multiple anonymous targets is focused on in this chapter. To recognize the targets, a simple, yet useful algorithm is proposed.

First of all, we assume that $(\varphi_{i,n}, d_{i,n})$ is the *i-th* set of DOA and TOA measurement from target i to the sensor n, where $i = \{1, 2, \cdots, I\}$ ans $n = \{1, 2, \cdots, N\}$, as shown in Fig. 3.1. By using the trigonometry functions,

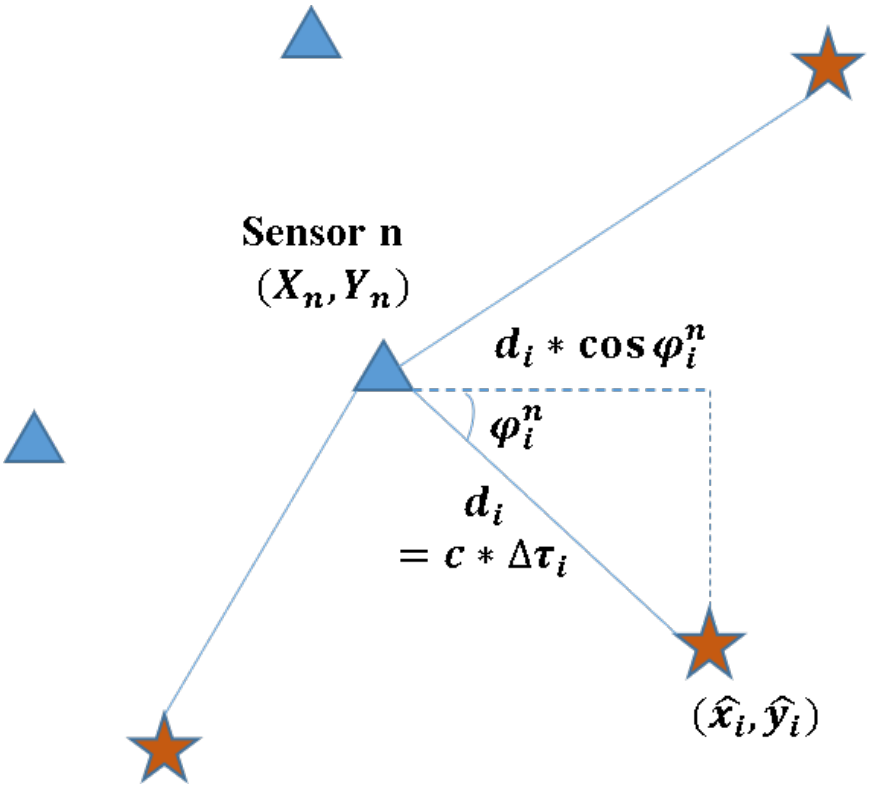

Figure 3.1: Sensor association in 2D scenario

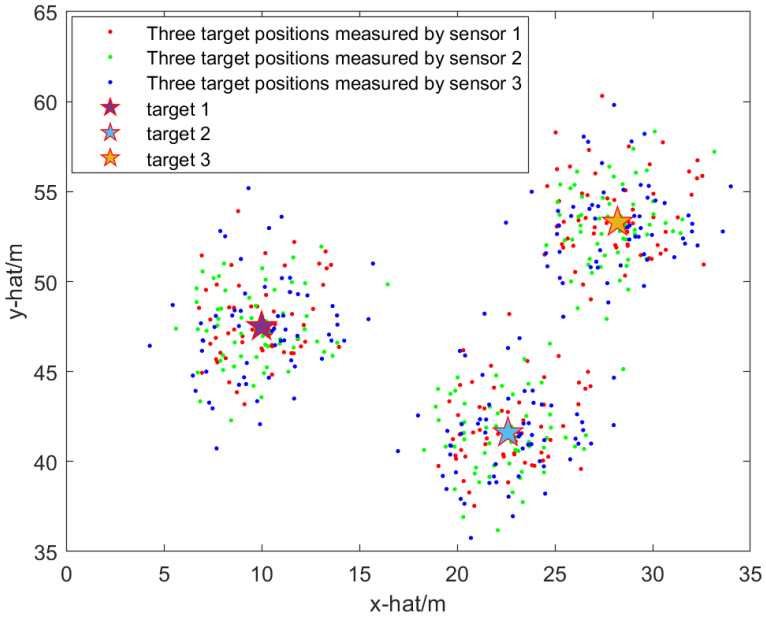

Figure 3.2: Rough estimates of targets

the rough estimate of the position can be calculated by

$$\begin{bmatrix} \hat{x}_{n,i} \\ \hat{y}_{n,i} \end{bmatrix} = \begin{bmatrix} d_{n,i} \times \cos\varphi_{n,i} \pm X_n \\ d_{n,i} \times \sin\varphi_{n,i} \pm Y_n \end{bmatrix}. \tag{3.5}$$

Let sensor n obtain L sets of DOA and TOA measurement from the target i. Each set of measurements is used to calculate the location information. Therefore, for sensor n, I clusters of targets are obtained. However, the position estimates obtained by (3.5) are unreliable because the estimation of $\widehat{x}$ and $\widehat{y}$ uses TOA and DOA observed by each sensor alone without message change over the FG. As shown in Fig. 3.2, the positions of the targets in each cluster are largely scattered.

Even though the initial position detection without using FG iteration is rough and the positions are scattered, we can identify which cluster the observations are in. This information makes the target-observation matching possible, and hence the measurement data can be properly input to the corresponding FG.

3.1.3 DOA-TOA Switching Algorithm

In this sub-chapter, the problem of positioning in certain critical situations is discussed. As show in Fig. 3.3(a), there may exist some sensors from

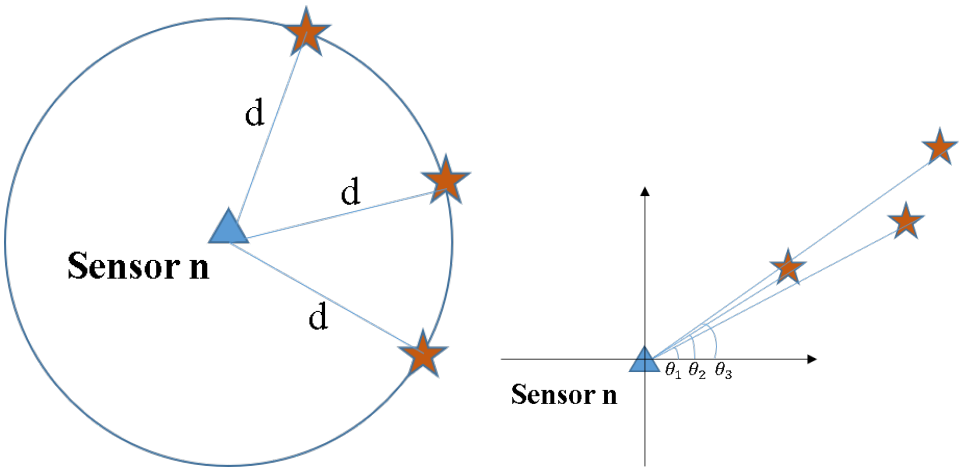

(a) The disadvantage of TOA (b) The disadvantage of DOA

Figure 3.3: The problem of positioning in certain situations

which multiple targets have the same distance to such sensors. In this case, TOA can not identify the positions accurately because the arriving time of the waves from the targets at such sensor are very close. On the other hand, there may exist some sensors when the multiple targets are on the same line originating from those sensors, or the angle differences are small, as shown in Fig. 3.3(b). In this case, DOA detection is unreliable.

Thus, a simple technique is proposed, which switches the use of either DOA or TOA. Assume that n-th sensor can obtain three measurement of DOA with mean and variance $(\varphi_{n,1}, \sigma_\varphi^2)$, $(\varphi_{n,2}, \sigma_\varphi^2)$ and $(\varphi_{n,3}, \sigma_\varphi^2)$. Calculate the relative angles by subtracting each of the two angles, and set the angle interval $[-k\sigma_\varphi, k\sigma_\varphi]$, where k is determined empirically. In this thesis, we set $k = 2$ to identify weather or not the measured DOAs are reliable. For the n-th sensor, TOA is used instead of DOA if one or some of the relative angles is/are within this interval. The pseudo code of proposed algorithm is shown in Algorithm 1, as below.

Algorithm 3.1 Switching algorithm

Initialization: φ_1, φ_2. φ_3 are the DOA measurement from target 1,2,3 to n-th sensor;

1: $\triangle\varphi_1 = \varphi_1 - \varphi_2$;
2: $\triangle\varphi_2 = \varphi_2 - \varphi_3$;
3: $\triangle\varphi_3 = \varphi_3 - \varphi_1$;
4: **if** $\triangle\varphi_1 \cup \triangle\varphi_2 \cup \triangle\varphi_3 \in [-k\sigma_\varphi, k\sigma_\varphi]$ **then**
5: Apply to TOA
6: **else**
7: Apply to DOA

3.1.4 Factor Graph-based Geolocation

The proposed joint DOA-TOA based FG is provided in this sub-chapter. The target index i and the sensor index n are omitted. In order to preserve the Gaussianity of the FG messages, the first order TS expansion centered at the point β, is used to approximate the true DOA and TOA information, expressed by equation (3.2) and equation (3.4), as

$$\varphi_k \approx h(\beta) + \frac{\partial h(\varphi_k)}{\partial x_k}(x_k - \beta_x) + \frac{\partial h(\varphi_k)}{\partial y_k}(y_k - \beta_y) \tag{3.6}$$

and

$$d_{2D,k} \approx q(\beta) + \frac{\partial q(d_{2D,k})}{\partial x_k}(x_k - \beta_x) + \frac{\partial q(d_{2D,k})}{\partial y_k}(y_k - \beta_y) \tag{3.7}$$

with $\beta = [\beta_x, \beta_y]^T$. To achieve simple, yet accurate approximation, let β be equal to predicted state $\mathbf{s}_{k|k-1}$, which is determined by the previous state. Then, the true DOA φ_k can be approximated as

$$\varphi_k \approx \lambda_1 x + \lambda_2 y + \lambda_3, \tag{3.8}$$

where λ_1, λ_2 and λ_3 are the constants, given by

$$\lambda_1 = \frac{Y - y_{k|k-1}}{(X - x_{k|k-1})^2 + (Y - y_{k|k-1})^2}, \tag{3.9}$$

$$\lambda_2 = \frac{-(X - x_{k|k-1})}{(X - x_{k|k-1})^2 + (Y - y_{k|k-1})^2}, \tag{3.10}$$

$$\begin{aligned}\lambda_3 =& \frac{(X - x_{k|k-1})y_{k|k-1} - (Y - y_{k|k-1})x_{k|k-1}}{(X - x_{k|k-1})^2 + (Y - y_{k|k-1})^2} \\ &+ \arctan\left(\frac{Y - y_{k|k-1}}{X - x_{k|k-1}}\right).\end{aligned} \tag{3.11}$$

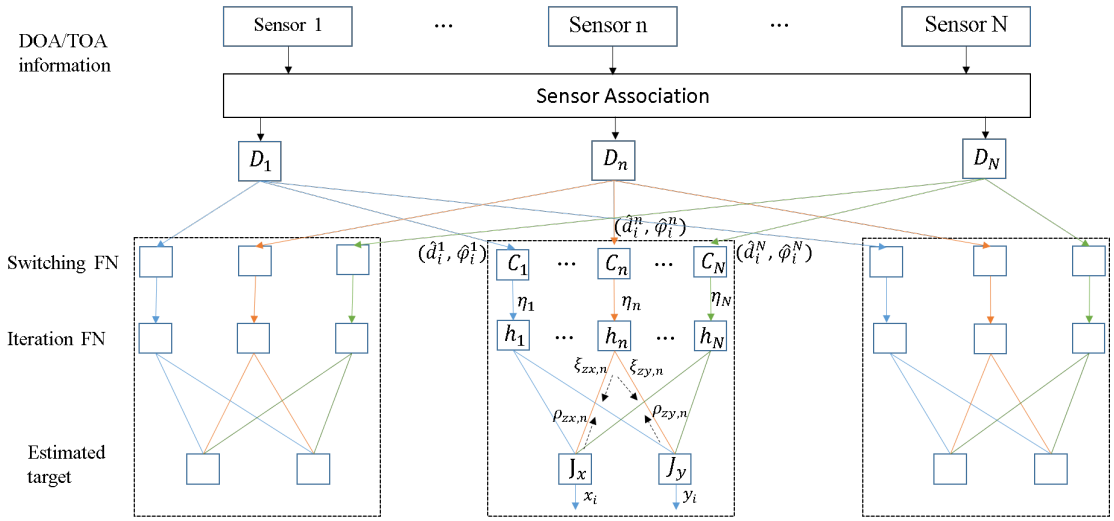

Figure 3.4: Proposed FG-GE in 2D scenario

The target position can then be derived as:

$$x = \frac{\varphi_k - \lambda_2 y - \lambda_3}{\lambda_1}, \tag{3.12}$$

$$y = \frac{\varphi_k - \lambda_1 x - \lambda_3}{\lambda_2}. \tag{3.13}$$

In the same way as in DOA, the true TOA $d_{2D,k}$ can be approximated as

$$d_{2D,k} = \tau_1 x + \tau_2 y + \tau_3, \tag{3.14}$$

where τ_1, τ_2 and τ_3 are the constants, given by

$$\tau_1 = \frac{-(X - x_{k|k-1})}{\sqrt{(X - x_{k|k-1})^2 + (Y - y_{k|k-1})^2}}, \tag{3.15}$$

$$\tau_2 = \frac{-(Y - y_{k|k-1})}{\sqrt{(X - x_{k|k-1})^2 + (Y - y_{k|k-1})^2}}, \tag{3.16}$$

$$\begin{aligned}\tau_3 =& \frac{(Y - y_{k|k-1})y_{k|k-1} + (X - x_{k|k-1})x_{k|k-1}}{\sqrt{(X - x_{k|k-1})^2 + (Y - y_{k|k-1})^2}} \\ &+ \sqrt{(X - x_{k|k-1})^2 + (Y - y_{k|k-1})^2}.\end{aligned} \tag{3.17}$$

Therefore, the target position can be derived by

$$x = \frac{d_{2D,k} - \tau_2 y - \tau_3}{\tau_1}, \tag{3.18}$$

$$y = \frac{d_{2D,k} - \tau_1 x - \tau_3}{\tau_2}. \tag{3.19}$$

The FG for the positions detection is illustrated in Fig. 3.4. Due to the space limitation, only one target position is estimated through the proposed FG. The positions of the rest of the targets can be obtained in the same way. First of all, the multiple targets are recognized by using the proposed sensor association. After the sensor association process, the measured DOA and TOA messages are calculated by the measurement function node (FN) D_n. The calculated mean and variance, i.e., $(m_{\varphi,n},\ \sigma^2_{\varphi,n})$ and $(m_{d,n},\ \sigma^2_{d,n})$, are passed through DOA-TOA switching FN C_n. In this node, either DOA or TOA message is selected, according to Algorithm 1, and is sent to the iteration FN. Let η_n denote the DOA or TOA message from the DOA-TOA switching FN. Let $\xi_{j_{x,n}}$ and $\xi_{j_{y,n}}$ denote downward messages from the iteration FN h_n to the estimated target FN J_x and J_y, respectively. Then, $\rho_{j_{x,n}}$ and $\rho_{j_{y,n}}$ are the upward messages from J_x and J_y to h_n, respectively. If the DOA measurement is selected by node C_n, η_n denotes the DOA message, i.e., $(m_{\varphi,n},\ \sigma^2_{\varphi,n})$. Otherwise, $(m_{d,n},\ \sigma^2_{d,n})$ denotes the mean and the variance of the TOA message. According to equations (3.8 - 3.13) and equations (3.15 - 3.19), the iteration process of DOA messages is described as follows.

- Update of downward messages:

$$m_{\xi_{j_{x,n}}} = \frac{1}{\lambda_{1,n}} m_{\eta_n} - \frac{\lambda_{2,n}}{\lambda_{1,n}} m_{\rho_{j_{y,n}}} - \frac{\lambda_{3,n}}{\lambda_{1,n}}, \tag{3.20}$$

$$\sigma^2_{\xi_{j_{x,n}}} = \frac{1}{\lambda^2_{1,n}} \sigma^2_{\eta_n} + \left(\frac{\lambda_{2,n}}{\lambda_{1,n}}\right)^2 \sigma^2_{\rho_{j_{y,n}}}, \tag{3.21}$$

$$m_{\xi_{j_{y,n}}} = \frac{1}{\lambda_{2,n}} m_{\eta_n} - \frac{\lambda_{1,n}}{\lambda_{2,n}} m_{\rho_{j_{x,n}}} - \frac{\lambda_{3,n}}{\lambda_{2,n}}, \tag{3.22}$$

$$\sigma^2_{\xi_{j_{y,n}}} = \frac{1}{\lambda^2_{2,n}} \sigma^2_{\eta_n} + \left(\frac{\lambda_{1,n}}{\lambda_{2,n}}\right)^2 \sigma^2_{\rho_{j_{x,n}}}. \tag{3.23}$$

  If the TOA measurement is selected by the node C_n, η_n denotes the TOA message, i.e., $(m_{d,n},\ \sigma^2_{d,n})$, where only the constants λ_1, λ_2 and λ_3 are replaced by the constants τ_1, τ_2 and τ_3.

- Update of upward messages:

$$\frac{1}{\sigma^2_{\rho_{j_{x,n}}}} = \sum_{i=1, i\neq n}^{N} \frac{1}{\sigma^2_{\xi_{j_{x,i}}}}, \tag{3.24}$$

$$m_{\rho_{j_{x,n}}} = \sigma^2_{\rho_{j_{x,n}}} \cdot \sum_{i=1, i\neq n}^{N} \frac{m_{\xi_{j_{x,i}}}}{\sigma^2_{\xi_{j_{x,i}}}}, \tag{3.25}$$

$$\frac{1}{\sigma^2_{\rho_{j_y,n}}} = \sum_{i=1, i\neq n}^{N} \frac{1}{\sigma^2_{\xi_{j_y,i}}}, \tag{3.26}$$

and

$$m_{\rho_{j_y,n}} = \sigma^2_{\rho_{j_y,n}} \cdot \sum_{i=1, i\neq n}^{N} \frac{m_{\xi_{j_y,i}}}{\sigma^2_{\xi_{j_y,i}}}. \tag{3.27}$$

The iteration is performed until convergence or until the maximum iteration time is reached. Finally, the estimated position is obtained by (m_{j_x}, m_{j_y}), which can be given by

$$\frac{1}{\sigma^2_{j_x}} = \sum_{i=1}^{N} \frac{1}{\sigma^2_{\xi_{j_x,i}}}, \tag{3.28}$$

$$\frac{1}{\sigma^2_{j_y}} = \sum_{i=1}^{N} \frac{1}{\sigma^2_{\xi_{j_y,i}}}, \tag{3.29}$$

$$m_{j_x} = \sigma^2_{j_x} \cdot \sum_{i=1}^{N} \frac{m_{\xi_{j_x,i}}}{\sigma^2_{\xi_{j_x,i}}}, \tag{3.30}$$

and

$$m_{j_y} = \sigma^2_{j_y} \cdot \sum_{i=1}^{N} \frac{m_{\xi_{j_y,i}}}{\sigma^2_{\xi_{j_y,i}}}. \tag{3.31}$$

3.1.5 Simulation Results

In this sub-chapter, results of a series of simulations conducted to evaluate the proposed FG-GE algorithms in the 2D, three targets scenario are presented.

The positions of three targets were set at (10, 47.5), (22.6, 41.6) and (28.2, 53.3). Three sensors were located at (-20, -10), (45, 110) and (100, 30). In the 2D geolocation, number of the sensors needed to identify the positions of the targets is common, regardless of how many targets exist. This is because the sensor association makes FGs for each target independent. As shown in Fig. 3.4, at least three sensors are need to exchange the messages in each FG. According to the assumptions discussed before, the measured DOAs and TOAs suffer from wihte Gaussian error. Let sensors obtain 60 DOA and TOA samples having standard deviation $\sigma_\varphi = 3^\circ$ and $\sigma_d = 15$ (meter), respectively. Let the maximum iteration time $J = 10$. The convergence behavior is shown in Fig. 3.5, with the initial guess was set at (0, 0). It can

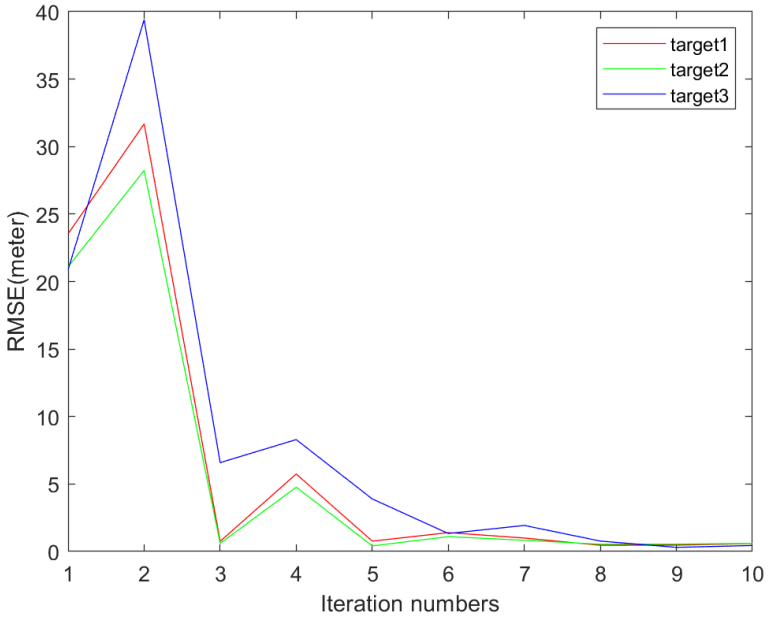

Figure 3.5: Convergence performance of FG-GE in 2D scenario

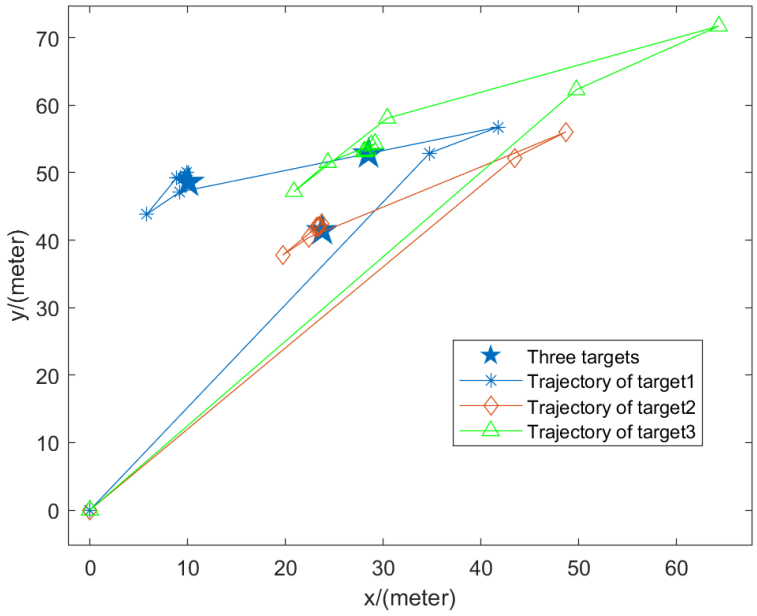

Figure 3.6: Trajectories of three targets with 3 sensors and 10 iterations

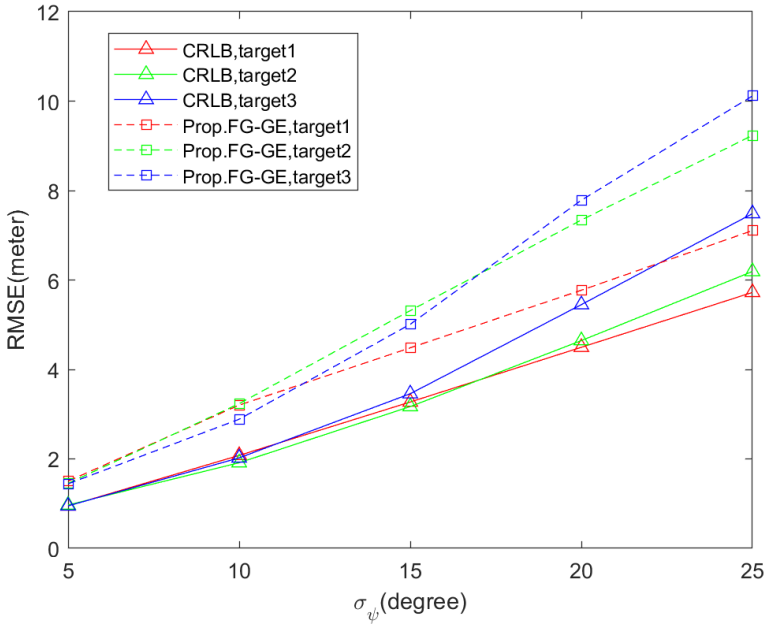

Figure 3.7: Comparison between the average RMSE and the CRLB

be found that even the initial guess is very far away form the 3 targets, with 7 or 8 iterations, they converge into the points very close to the true targets positions. Moreover, the trajectories of three targets with 10 iterations are shown in Fig. 3.6.

The performance accuracy of the proposed FG-GE algorithm is evaluated by comparing the average Root Mean Square Error (RMSE) with the CRLB. The result is shown in Fig. 3.7. Obviously, the gaps between the average RMSE obtained by the simulations and the CRLBs are very small, especially in the value range of small σ_φ.

3.2 Multi-target Position Detection in 3D scenario

3.2.1 System Model

In the 3D scenario, φ_n is the same measurement as in the X-Y plane expressed by equation (3.1). Another measurement of DOA θ, as shown in Fig. 3.8, is the elevation angle given by

$$\widehat{\theta}_{n,k} = h(\theta_{n,k}) + u_{\theta,n,k} \tag{3.32}$$

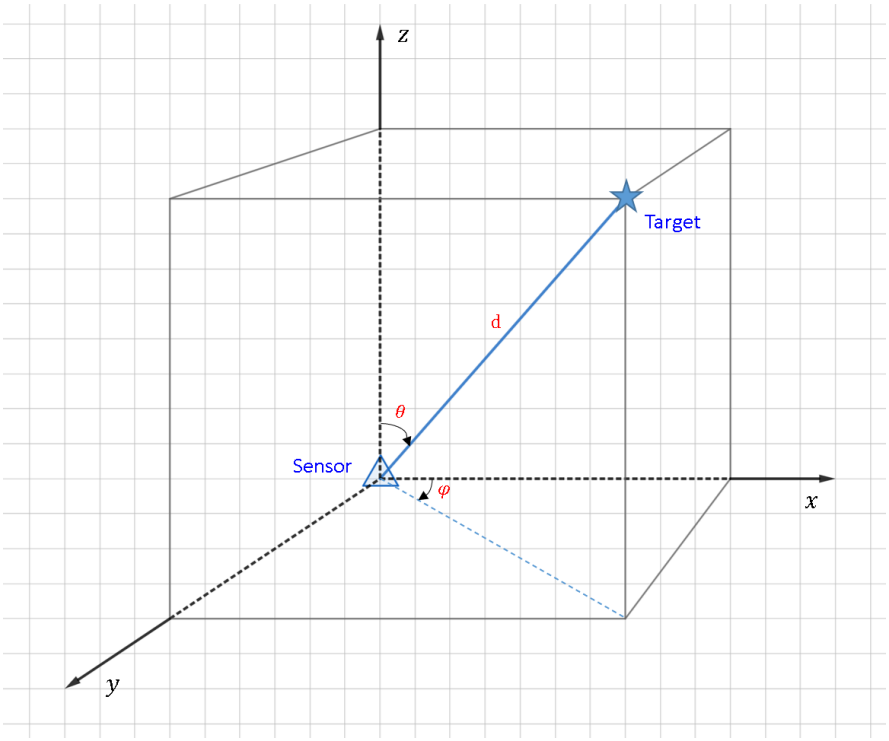

Figure 3.8: System model in 3D scenario

at timing k, with $u_{\theta,n,k} \sim \mathcal{N}\ (0, \sigma_\theta^2)$ the measurement error. The true DOA $h(\theta_{n,k})$ is given by

$$h(\theta_{n,k}) = \arctan\left(\frac{\sqrt{(Y_n - y_k)^2 + (X_n - x_k)^2}}{Z_n - z_k}\right). \tag{3.33}$$

The measurement of TOA in the 3D scenario is given by

$$\widehat{d}_{3D,n,k} = \sqrt{(X_n - x_k)^2 + (Y_n - y_k)^2 + (Z_n - z_k)^2} + v_{3D,n,k} \tag{3.34}$$

with $v_{3D,n,k} \sim \mathcal{N}\ (0, \sigma_d^2)$ the measurement error.

3.2.2 Sensor Association

In the 3D scenario, the sensor association is also used to solve the matching problem between the multiple distributed sensors and anonymous targets. Similarly to the 2D scenario, by using the trigonometric functions, the rough

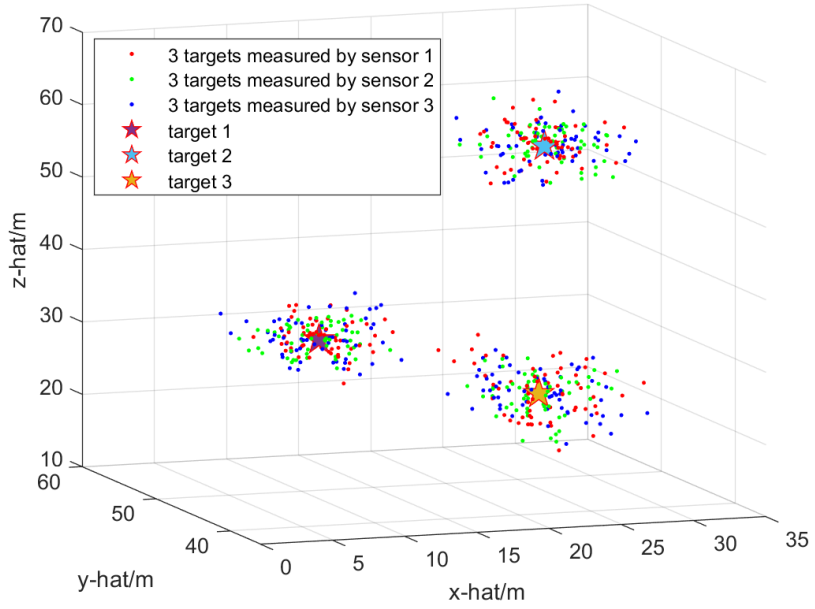

Figure 3.9: Rough estimates of the targets in 3D scenario

estimates of the targets can be given by

$$\begin{bmatrix} \hat{x}_{n,i} \\ \hat{y}_{n,i} \\ \hat{z}_{n,i} \end{bmatrix} = \begin{bmatrix} d_{n,i} \times \sin\theta_{n,i} \times \cos\varphi_{n,i} \pm X_n \\ d_{n,i} \times \cos\theta_{n,i} \times \sin\varphi_{n,i} \pm Y_n \\ d_{n,i} \times \cos\theta_{n,i} \pm Z_n \end{bmatrix}. \tag{3.35}$$

As shown in Fig.3.9, the positions in each cluster are also largely scattered because of the same reason as in the 2D case.

3.2.3 Projection Algorithm

In this sub-chapter, the proposed geolocation technique in the 3D scenario is described. In the 3D scenario, since the situation where the multiple targets are on the same line originating from a sensor rarely exists, the DOA-TOA switching algorithm is omitted. This sub-chapter proposes a technique for estimating the multi-target positions, which can be performed using three projected 2D FGs.

First of all, we project the target onto the Y-Z and X-Z planes as shown in Fig.3.10. To combine the three projected 2D FGs for identifying target position, we need the angle information on the projected plane between the projected point and each sensor. Assume that sensors can measure the

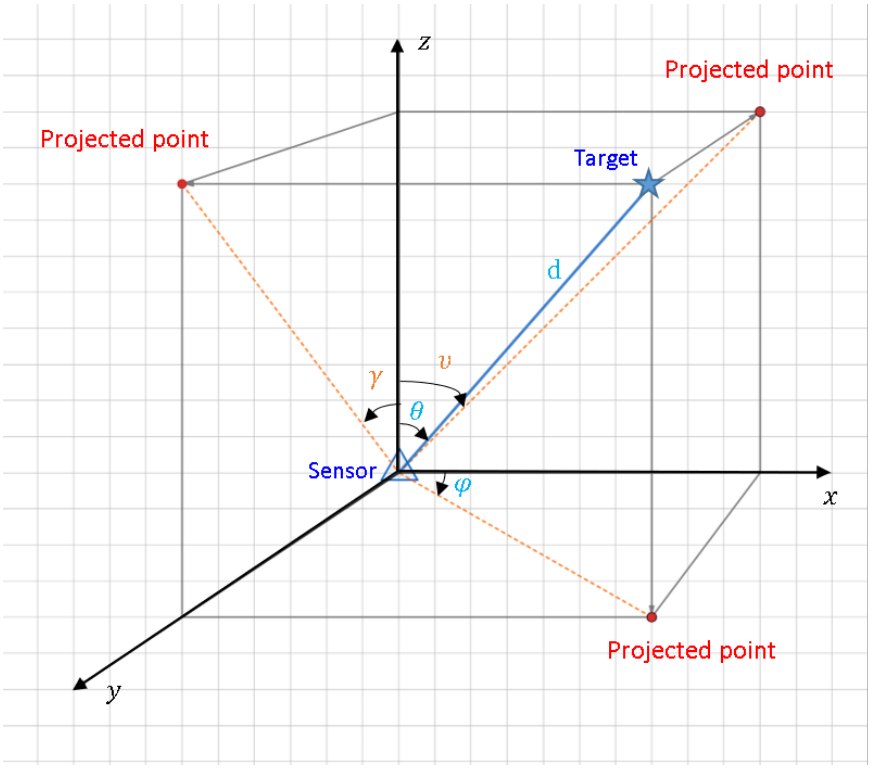

Figure 3.10: Projection onto 2D planes

azimuth angle φ, the elevation angle θ and the relative distance d based on equations (3.1), (3.32) and (3.34). The relative distance in the (X, Y, Z) coordinate can be calculated as

$$\begin{bmatrix} \triangle x \\ \triangle y \\ \triangle z \end{bmatrix} = \begin{bmatrix} d \times \sin\theta \times \cos\varphi \\ d \times \cos\theta \times \sin\varphi \\ d \times \cos\theta \end{bmatrix}. \tag{3.36}$$

The tangent of the angle υ between the projected point (x, z) and the sensor is given by

$$\tan\upsilon = \frac{\triangle x}{\triangle z} = \tan\theta \cdot \cos\varphi. \tag{3.37}$$

The tangent of the angle γ between the projection point (y, z) and the sensor is given by

$$\tan\gamma = \frac{\triangle y}{\triangle z} = \tan\theta \cdot \sin\varphi. \tag{3.38}$$

The mean and the variance of the product of two independent Gaussian random variables, $a \sim \mathcal{N}(m_a, \sigma_a^2)$ and $b \sim \mathcal{N}(m_b, \sigma_b^2)$, can be given by

$$m_{a \cdot b} = m_a \cdot m_b, \tag{3.39}$$

$$\sigma_{a\cdot b}^2 = m_a^2 \cdot \sigma_b^2 + m_b^2 \cdot \sigma_a^2 + \sigma_a^2 \cdot \sigma_b^2, \tag{3.40}$$

where $a, b \in \{\tan\theta, \cos\varphi\}$ or $\{\tan\theta, \sin\varphi\}$. It should be noted that equations (3.37) and (3.38) are nonlinear function which does not allow us to use the Gaussian assumption of the messages in FG. Therefore, the first-order TS expansion is applied to approximate the trigonometric functions as,

$$f(\alpha) \approx f(m_\alpha) + f'(m_\alpha)(\alpha - m_\alpha), \tag{3.41}$$

where $f(\alpha)$ is either $\tan\theta$, $\cos\varphi$ or $\sin\varphi$, and $f(m_\alpha)$ is either $\tan(m_\theta)$, $\cos(m_\varphi)$ or $\sin(m_\varphi)$. Then, the mean and the variance $(m_{f(\alpha)}, \sigma_{f(\alpha)}^2)$ can be given by

$$m_{f(\alpha)} \approx f(m_\alpha), \tag{3.42}$$

$$\sigma_{f(\alpha)}^2 \approx [f'(m_\alpha)]^2 \cdot \sigma_\alpha^2. \tag{3.43}$$

The mean and the variance of the trigonometric function calculated from equations (3.42) and (3.43) are summarized in TABLE 3.1.

Table 3.1: Approximated means and variances of related trigonometric functions

	Approximated mean	Approximated variance
$\tan(\alpha)$	$\tan(m_\alpha)$	$\sec^4(m_\alpha) \cdot\sigma_\alpha^2$
$\sin(\alpha)$	$\sin(m_\alpha)$	$\cos^2(m_\alpha) \cdot\sigma_\alpha^2$
$\cos(\alpha)$	$\cos(m_\alpha)$	$\sin^2(m_\alpha) \cdot\sigma_\alpha^2$

With the approximation described above, the tangent of the angle υ can further be expressed as

$$m_{\tan(\upsilon)} = m_{\tan(\theta)} \cdot m_{\cos(\varphi)}, \tag{3.44}$$

$$\sigma_{\tan(\upsilon)}^2 = m_{\tan(\theta)}^2 \sigma_{\sin(\varphi)}^2 + m_{\sin(\varphi)}^2 \sigma_{\tan(\theta)}^2 + \sigma_{\tan(\theta)}^2 \sigma_{\sin(\varphi)}^2. \tag{3.45}$$

Again, by using equations (3.42) and (3.43), the mean and the variance of υ can be obtained by

$$m_\upsilon \approx \arctan(m_{\tan(\upsilon)}), \tag{3.46}$$

$$\sigma_\upsilon^2 \approx \frac{\sigma_{\tan(\upsilon)}^2}{\sec^4(m_\upsilon)}. \tag{3.47}$$

The mean and the variance of angle γ can also be calculated in the same way.

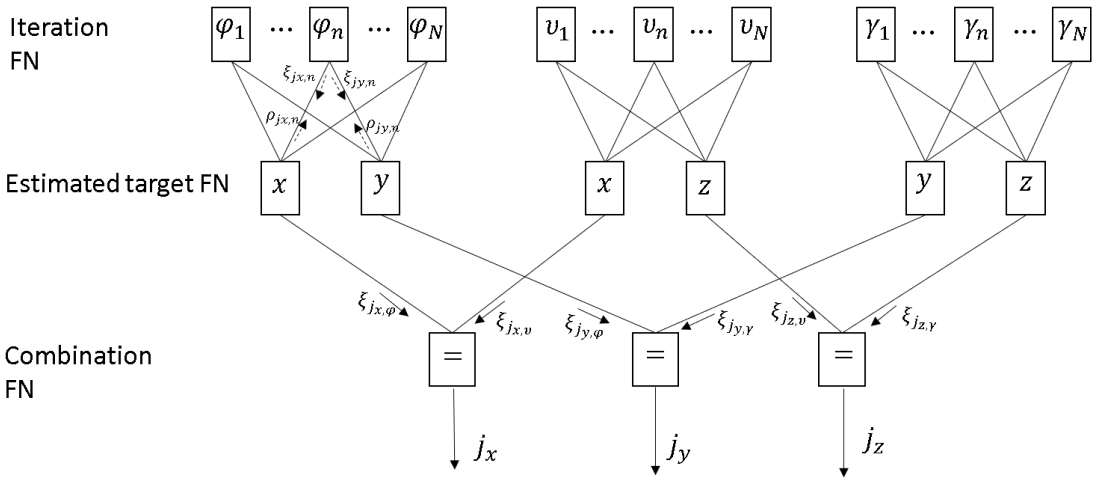

Figure 3.11: Proposed FG-GE in 3D scenario

3.2.4 Factor Graph-based Geolocation

In the same way as the proposed FG algorithm in the 2D scenario was derived, we apply the first-order TS expansion to approximate the true DOA φ_k, υ_k and γ_k at the timing k. Since φ_k has been discussed in the 2D scenario, only υ_k and γ_k are discussed in this sub-chapter. Note that the true DOA υ_k and γ_k are given by

$$\upsilon_k = \arctan\left(\frac{X - x_{\upsilon,k}}{Z - z_{\upsilon,k}}\right), \tag{3.48}$$

$$\gamma_k = \arctan\left(\frac{Y - y_{\upsilon,k}}{Z - z_{\upsilon,k}}\right). \tag{3.49}$$

By using the first-order TS expansion to approximate equation (3.48), centered at the point $s_{\upsilon,k|k-1}$, υ_k can further be expressed as

$$\upsilon_k \approx a_1 x_{\upsilon,k} + a_2 z_{\upsilon,k} + a_3, \tag{3.50}$$

where

$$a_1 = \frac{-(Z - z_{\upsilon,k|k-1})}{(Z - z_{\upsilon,k|k-1})^2 + (X - x_{\upsilon,k|k-1})^2}, \tag{3.51}$$

$$a_2 = \frac{X - x_{\upsilon,k|k-1}}{(Z - z_{\upsilon,k|k-1})^2 + (X - x_{\upsilon,k|k-1})^2}, \tag{3.52}$$

$$
\begin{aligned}
a_3 =& \frac{(Z - z_{\upsilon,k|k-1})x_{\upsilon,k|k-1} - (X - x_{\upsilon,k|k-1})z_{\upsilon,k|k-1}}{(Z - z_{\upsilon,k|k-1})^2 + (X - x_{\upsilon,k|k-1})^2} \\
&+ \arctan\left(\frac{X - x_{\upsilon,k|k-1}}{Z - z_{\upsilon,k|k-1}}\right).
\end{aligned} \tag{3.53}
$$

Therefore, the target position can be expressed as

$$
x_{\upsilon,k} = \frac{\upsilon_k - a_2 z_{\upsilon,k} - a_3}{a_1}, \tag{3.54}
$$

$$
z_{\upsilon,k} = \frac{\upsilon_k - a_1 x_{\upsilon,k} - a_3}{a_2}. \tag{3.55}
$$

Similarly, γ_k can be expressed as

$$
\gamma_k \approx b_1 y_{\gamma,k} + b_2 z_{\gamma,k} + b_3, \tag{3.56}
$$

where

$$
b_1 = \frac{-(Z - z_{\gamma,k|k-1})}{(Z - z_{\gamma,k|k-1})^2 + (Y - y_{\gamma,k|k-1})^2}, \tag{3.57}
$$

$$
b_2 = \frac{Y - y_{\gamma,k|k-1}}{(Z - z_{\gamma,k|k-1})^2 + (Y - y_{\gamma,k|k-1})^2}, \tag{3.58}
$$

$$
\begin{aligned}
b_3 =& \frac{(Z - z_{\gamma,k|k-1})y_{\gamma,k|k-1} - (Y - y_{\gamma,k|k-1})z_{\gamma,k|k-1}}{(Z - z_{\gamma,k|k-1})^2 + (Y - y_{\gamma,k|k-1})^2} \\
&+ \arctan\left(\frac{Y - y_{\gamma,k|k-1}}{Z - z_{\gamma,k|k-1}}\right).
\end{aligned} \tag{3.59}
$$

The target position can then be expressed by

$$
y_{\gamma,k} = \frac{\gamma_k - b_2 z_{\gamma,k} - b_3}{b_1}, \tag{3.60}
$$

$$
z_{\gamma,k} = \frac{\gamma_k - b_1 y_{\gamma,k} - b_3}{b_2}. \tag{3.61}
$$

According to equations (3.8) - (3.13) and equations (3.48) - (3.61), the FG-GE in 3D (3D FG-GE) using the three projected planes is illustrated in Fig.3.11. A new function node, combination function node, is introduced between iteration function node and estimated target function node. In the combination function node, the fact that the product of two independent Gaussian PDFs, following $\mathcal{N}(m_a, \sigma_a^2)$ and $\mathcal{N}(m_b, \sigma_b^2)$, becomes also Gaussian PDF with $\mathcal{N}\left(\frac{m_a\sigma_b^2 + m_b\sigma_a^2}{\sigma_a^2 + \sigma_b^2}, \frac{1}{\frac{1}{\sigma_a^2} + \frac{1}{\sigma_b^2}}\right)$ is used. Therefore, the means and the

variances of the message for the combination function node can be calculated by

$$m_{j_x} = \frac{m_{\xi_{j_x,\varphi}} \cdot \sigma^2_{\xi_{j_x,\upsilon}} + m_{\xi_{j_x,\upsilon}} \cdot \sigma^2_{\xi_{j_x,\varphi}}}{\sigma^2_{\xi_{j_x,\varphi}} + \sigma^2_{\xi_{j_x,\upsilon}}}, \tag{3.62}$$

$$m_{j_y} = \frac{m_{\xi_{j_y,\varphi}} \cdot \sigma^2_{\xi_{j_y,\gamma}} + m_{\xi_{j_y,\gamma}} \cdot \sigma^2_{\xi_{j_y,\varphi}}}{\sigma^2_{\xi_{j_y,\varphi}} + \sigma^2_{\xi_{j_y,\gamma}}}, \tag{3.63}$$

$$m_{j_z} = \frac{m_{\xi_{j_z,\upsilon}} \cdot \sigma^2_{\xi_{j_z,\gamma}} + m_{\xi_{j_z,\gamma}} \cdot \sigma^2_{\xi_{j_z,\upsilon}}}{\sigma^2_{\xi_{j_z,\upsilon}} + \sigma^2_{\xi_{j_z,\gamma}}}, \tag{3.64}$$

and

$$\sigma^2_{j_x} = \frac{1}{\frac{1}{\sigma^2_{\xi_{j_x,\varphi}}} + \frac{1}{\sigma^2_{\xi_{j_x,\upsilon}}}}, \tag{3.65}$$

$$\sigma^2_{j_y} = \frac{1}{\frac{1}{\sigma^2_{\xi_{j_y,\varphi}}} + \frac{1}{\sigma^2_{\xi_{j_y,\gamma}}}}, \tag{3.66}$$

$$\sigma^2_{j_z} = \frac{1}{\frac{1}{\sigma^2_{\xi_{j_z,\upsilon}}} + \frac{1}{\sigma^2_{\xi_{j_z,\gamma}}}}. \tag{3.67}$$

3.2.5 Simulation Results

As mentioned before, in the 3D scenario, elevation angle θ is assumed to be obtained from the distributed sensors. Since the disadvantageous situations of TOA-only or DOA-only rarely occur in 3D scenario, the FG-GE based on the DOA-only is utilized in the simulation, and the switching algorithm is omitted.

All other parameters are the same as the 2D's case, except that the positions of the distributed sensors and the initial target points were changed: the three distributed sensors were located at (-20, -30, -10), (45, 110, 55) and (100, 30, 60). In 3D geolocation, also three sensors are needed regardless of target numbers. This is because with the proposed technique, 3D geolocation is decomposed into three 2D FG-based geolocations. The initial points of three targets were set at (10, 47.5, 12), (22.6, 41.6, 65) and (48.2, 53.3, 80). We assume that each sensor can obtain 60 samples of azimuth φ and elevation θ, with $\sigma_\varphi = \sigma_\theta = 3^\circ$. The accuracy of the proposed 3D FG-GE was evaluated by changing σ_φ and σ_θ values. It should be noted that σ_φ and σ_θ may differ among the distributed sensors in practice. However, in the simulation, we assume that the DOA measurements of all sensors have the same standard deviation. Therefore, we set $\sigma_\varphi = \sigma_\theta$. It is found from Fig.

3.12 that the average RMSEs of the three targets are small, especially when σ_φ and σ_θ values are in a small value range.

Moreover, we compared the proposed technique with conventional linear least-square (LS) detection algorithm to evaluate the performance. As in [34], the position estimate $[m_x, m_y, m_z]$ of the LS algorithm is given by

$$\begin{bmatrix} m_x \\ m_y \\ m_z \end{bmatrix} = (\mathbf{U}^T\mathbf{U})^{-1}\mathbf{U}^T\mathbf{V}, \tag{3.68}$$

where $\mathbf{U} = [U_1, U_2, \cdots, U_N]^T$ and $\mathbf{V} = [V_1, V_2, \cdots, V_N]^T$. It should be noted that the sensor index is omitted for simplicity. The vector $\mathbf{U}$ and $\mathbf{V}$ are given by

$$U = \begin{bmatrix} -\cot(m_\varphi) & 1 & 0 \\ 1 & 0 & -\sin(m_\varphi)\tan(m_\theta) \\ 0 & 1 & -\cos(m_\varphi)\tan(m_\theta) \end{bmatrix}, \tag{3.69}$$

$$V = \begin{bmatrix} Y - X\cot(m_\varphi) \\ X - Z\sin(m_\varphi)\tan(m_\theta) \\ Y - Z\cos(m_\varphi)\tan(m_\theta) \end{bmatrix}. \tag{3.70}$$

As shown in Fig. 3.13, it is obvious that the proposed technique has more accurate performance than conventional linear LS detection algorithm.

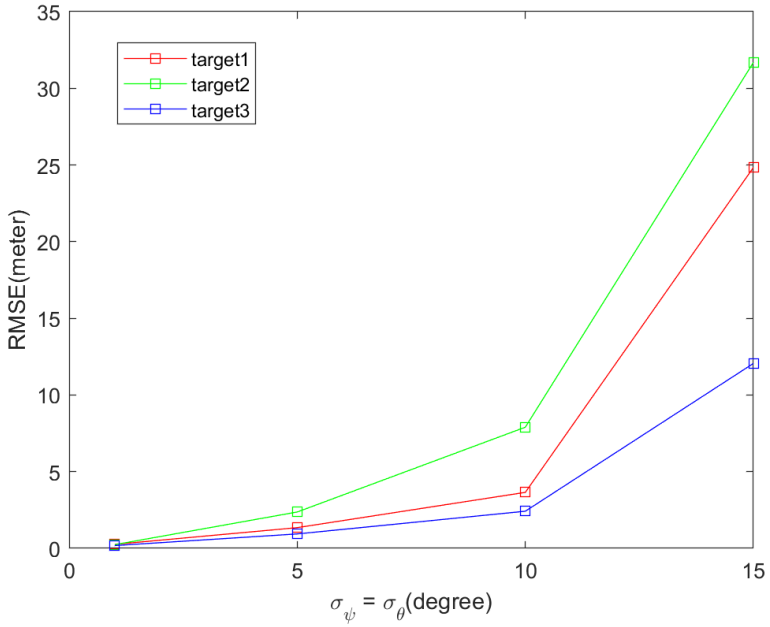

Figure 3.12: Average RMSE versus variance for FG-GE in 3D scenario

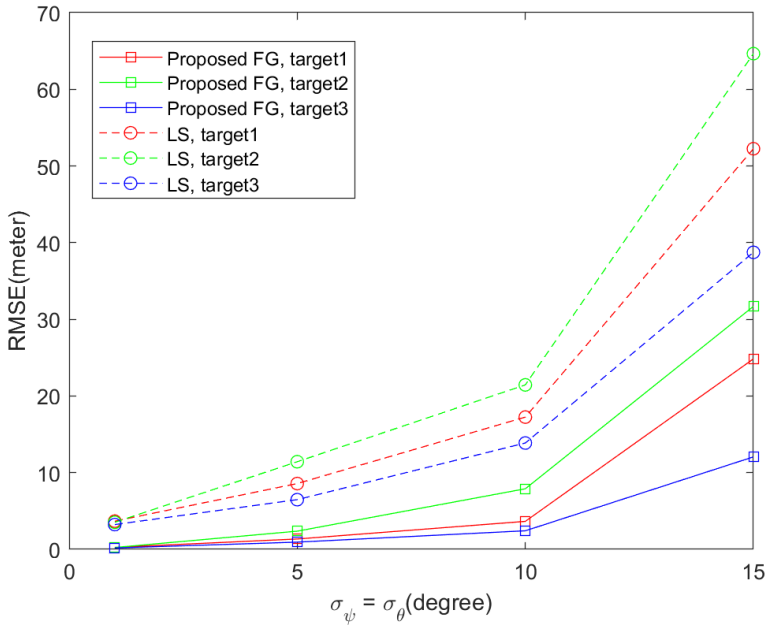

Figure 3.13: Average RMSE comparison between FG and LS in 3D scenario

Chapter 4

Factor Graph-based Tracking

In this chapter, FG-based tracking algorithm with EKF is proposed to track the multi-target trajectories in the 2D and 3D scenarios. The detailed techniques are described in the following sub-chapters. The simulations of two scenarios are also provided to evaluate the performance of the tracking algorithm.

4.1 System Model

For the tracking system, the multi-target non-linear discrete state-space model (SSM) is used, as in [35]. I anonymous target positions are located in $\mathbf{s}_k = [x_k, y_k]^T$ or $\mathbf{s}_k = [x_k, y_k, z_k]^T$ at timing k in the 2D and 3D scenarios, respectively. The SSM equation is given by

$$\mathbf{s}_k = f(\mathbf{s}_{k-1}) + \mathbf{w}_k, \tag{4.1}$$

where $f(\cdot)$ is a non-linear function, and $\mathbf{w}_k = [w_{x,k}, w_{y,k}]^T$ or $\mathbf{w}_k = [w_{x,k}, w_{y,k}, w_{z,k}]^T$ the white Gaussian noise vector in the 2D and 3D scenarios, respectively. In order to keep the Gaussianity of the messages in the FG, the first order Taylor series (TS) expansion needs to be used to approximate $f(\cdot)$ by a linear function. The first order TS is given by

$$f(\mathbf{s}_{k-1}) \approx f(\alpha) + f'(\alpha)(\mathbf{s}_{k-1} - \alpha), \tag{4.2}$$

where α is the center point of the TS expansion, $f(\alpha)$ is the current position $\mathbf{s}_{k-1}$, and the first order derivative $f'(\alpha)(\mathbf{s}_{k-1} - \alpha) = \mathbf{v}_{k-1} \cdot \triangle t$ is the distance between s_{k-1} and s_k without loss of generality, we normalize $\triangle t = 1$. Then, equation (4.1) can be rewritten as

$$\mathbf{s}_k \approx \mathbf{s}_{k-1} + \mathbf{v}_{k-1} + \mathbf{w}_k. \tag{4.3}$$

The velocity $\mathbf{v}_{k-1}$ is updated by EKF. The observation state $\mathbf{j}_k$ is given by

$$\mathbf{j}_k = g(\mathbf{s}_k) + \mathbf{e}_k \tag{4.4}$$

with $\mathbf{e}_k \sim \mathcal{N}(0, \sigma_e^2)$ the observation noise. Since $\mathbf{e}_k$ is unknown, we use the variance of φ_k that achieves the smallest σ_e^2, which can be calculated from the CRLB [35].

4.2 Extend Kalman Filter

The objective of EKF is to find the maximum posterior probability $p(\mathbf{s}_k, \mathbf{v}_k|\mathbf{j}_{1:k})$, where subscript $1:k$ is the measurement data series from the timing 1 to k. As in [35], the posterior probability $p(\mathbf{s}_k, \mathbf{v}_k|\mathbf{j}_{1:k})$ can be given by

$$p(\mathbf{s}_k, \mathbf{v}_k|\mathbf{j}_{1:k}) = \sum_{\sim\mathbf{s}_k, \sim\mathbf{v}_k} p(\mathbf{s}_{1:k}, \mathbf{v}_{1:k}|\mathbf{j}_{1:k}), \tag{4.5}$$

where $\sim$ denotes the operator of the exclusion. According to Bayes's theorem, the joint distribution (4.5) can be further expressed as

$$p(\mathbf{s}_{1:k}, \mathbf{v}_{1:k}|\mathbf{j}_{1:k}) = \frac{p(\mathbf{j}_k|\mathbf{s}_{1:k}, \mathbf{v}_{1:k}, \mathbf{j}_{1:k-1})p(\mathbf{s}_{1:k}, \mathbf{v}_{1:k}, \mathbf{j}_{1:k-1})}{p(\mathbf{j}_{1:k})}. \tag{4.6}$$

Due to the fact that $\mathbf{j}_k$ is only determined by $\mathbf{s}_k$ and $p(\mathbf{j}_{1:k})$ is known and common to all the time index $1:k$, and hence can be omitted, equation (4.6) can be derived as

$$p(\mathbf{s}_{1:k}, \mathbf{v}_{1:k}|\mathbf{j}_{1:k}) \propto p(\mathbf{j}_k|\mathbf{s}_k)p(\mathbf{s}_{1:k}, \mathbf{v}_{1:k}, \mathbf{j}_{1:k-1}). \tag{4.7}$$

Furthermore,

$$\begin{aligned} &p(\mathbf{s}_{1:k}, \mathbf{v}_{1:k}, \mathbf{j}_{1:k-1}) \\ &= p(\mathbf{s}_k|\mathbf{s}_{k-1}, \mathbf{v}_{k-1})p(\mathbf{v}_k|\mathbf{v}_{k-1})p(\mathbf{s}_{1:k-1}, \mathbf{v}_{1:k-1}|\mathbf{j}_{1:k-1})p(\mathbf{j}_{1:k-1}) \\ &\propto p(\mathbf{s}_k|\mathbf{s}_{k-1}, \mathbf{v}_{k-1})p(\mathbf{v}_k|\mathbf{v}_{k-1})p(\mathbf{s}_{1:k-1}, \mathbf{v}_{1:k-1}|\mathbf{j}_{1:k-1}) \end{aligned} \tag{4.8}$$

where $\mathbf{j}_{1:k-1}$ is ignored hence only $\mathbf{s}_k$ is determined by $\mathbf{s}_{k-1}$ and $\mathbf{v}_{k-1}$. Further more, $\mathbf{v}_k$ is only determined by $\mathbf{v}_{k-1}$. $p(\mathbf{s}_{1:k-1}, \mathbf{v}_{1:k-1}|\mathbf{j}_{1:k-1})$ is recursively related to the state at the previous timing. Therefore, by combining equations (4.7) and (4.8), the posterior probability $p(\mathbf{s}_k, \mathbf{v}_k|\mathbf{j}_{1:k})$ can be derived as follow

$$\begin{aligned} &p(\mathbf{s}_{1:k}, \mathbf{v}_{1:k}|\mathbf{j}_{1:k}) \\ &\propto \prod_{1:k} p(\mathbf{s}_k|\mathbf{s}_{k-1}, \mathbf{v}_{k-1})p(\mathbf{v}_k|\mathbf{v}_{k-1})p(\mathbf{j}_k|\mathbf{s}_k). \end{aligned} \tag{4.9}$$

where $\prod$ represents timing series from 1 to k.

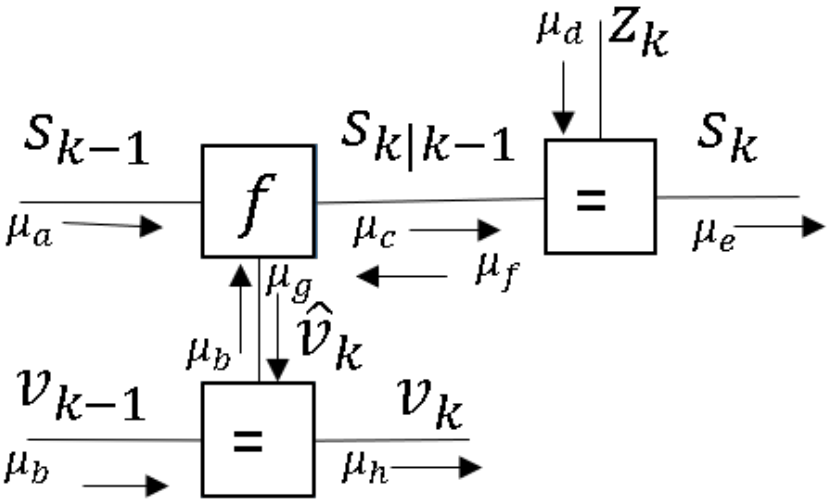

Figure 4.1: Proposed FG-GE-EKF

4.3 Factor Graph-based Tracking

In this sub-chapter, the FG for tracking based on EKF illustrated in Fig. 4.1. According to equation (4.9). The EKF process can be divided into 3 parts as follow.

4.3.1 State Prediction

Based on the outputs of FG-GE-EKF at previous timing $k-1$, the prediction message of the next state $\mathbf{s}_{k|k-1}$, as shown in Fig. 4.1, can be given by

$$\begin{aligned}&\mu_c(\mathbf{s}_{k|k-1})\\&=\sum_{\mathbf{s}_{k-1}}\sum_{\mathbf{v}_{k-1}} f(\mathbf{s}_{k|k-1}|\mathbf{s}_{k-1},\mathbf{v}_{k-1})\mu_a(\mathbf{s}_{k-1})\mu_b(\mathbf{v}_{k-1}),\end{aligned} \tag{4.10}$$

where the messages $\mu_a(\mathbf{s}_{k-1})$ and $\mu_b(\mathbf{v}_{k-1})$ are from previous state at the timing $k-1$, with the function $f(\mathbf{s}_{k|k-1}|\mathbf{s}_{k-1},\mathbf{v}_{k-1}) = \mathbf{s}_{k-1}+\mathbf{v}_{k-1}$. It should be noted that since the messages are assumed to be statically independent, the covariance matrix $\mathbf{P}_{k|k}$ in equations 2.13 - 2.15 is $\mathbf{I}$.

4.3.2 State Update

The current state can be obtained by using the current observation $\mathbf{j}_k$ to refine the state prediction $\mathbf{s}_{k|k-1}$, according to the EKF algorithm. Therefore, the

current state $\mathbf{s}_k$ can be given by

$$\mu_e(\mathbf{s}_k) = \mu_c(\mathbf{s}_{k|k-1})\mu_d(\mathbf{j}_k), \tag{4.11}$$

where $\mu_d(\mathbf{j}_k)$ is the observed value obtained by the proposed position detection FG.

4.3.3 Gradient Update

Since the gradient vector $\mathbf{v}_k$ is only determined by $\mathbf{v}_{k-1}$, we introduce the correction term $\hat{\mathbf{v}}_k$ to update $\mathbf{v}_k$. The correction term $\hat{\mathbf{v}}_k$ can be obtained by letting two adjacent locations be divided by unit time. Therefore, the message $\hat{\mathbf{v}}_k$ is given by

$$\mu_g(\hat{\mathbf{v}}_k) = \sum_{\mathbf{s}_{k-1}} \sum_{\mathbf{s}_k} f(\hat{\mathbf{v}}_k|\mathbf{s}_{k-1}, \mathbf{s}_k)\mu_a(\mathbf{s}_{k-1})\mu_f(\mathbf{s}_k), \tag{4.12}$$

where $\mu_f(\mathbf{s}_k)$ is the current state message, and the function $f(\hat{\mathbf{v}}_k|\mathbf{s}_{k-1}, \mathbf{s}_k) = \mathbf{s}_k - \mathbf{s}_{k-1}$. Then, the update of the gradient vector $\mathbf{v}_k$ can be obtained by

$$\mu_h(\mathbf{v}_k) = \mu_b(\mathbf{v}_{k-1})\mu_g(\hat{\mathbf{v}}_k). \tag{4.13}$$

4.3.4 Simulation Results in 2D scenario

In this sub-chapter, results of a series of simulations conducted to evaluate the proposed FG-GE-EKF algorithms in the 2D, three targets scenario are presented. The process equations used in the simulation for the three target case are shown as below:

$$x_{1,k} = x_{1,k-1} + \cos\left(\frac{x_{1,k-1}\Phi}{k}\right) + \omega_{x,k}, \tag{4.14}$$

$$y_{1,k} = y_{1,k-1} + \sin\left(\frac{x_{1,k-1}\Phi}{k}\right) + \omega_{y,k}, \tag{4.15}$$

$$x_{2,k} = x_{2,k-1} + \cos\left(0.2k\Phi\right) + \omega_{x,k}, \tag{4.16}$$

$$y_{2,k} = y_{2,k-1} + \sin\left(0.2k\Phi\right) + \omega_{y,k}, \tag{4.17}$$

$$x_{3,k} = x_{3,k-1} + (0.02k - 0.074) + \omega_{x,k}, \tag{4.18}$$

$$y_{3,k} = y_{3,k-1} + (0.03k - 0.074) + \omega_{y,k}, \tag{4.19}$$

where Φ was set at $\pi/10$ and the timing $k = \{1, 2, \cdots, 40\}$. The initial points of three targets were set at (10, 47.5), (22.6, 41.6) and (28.2, 53.3). Three sensors were located at (-20, -10), (45, 110) and (100, 30). At each timing,

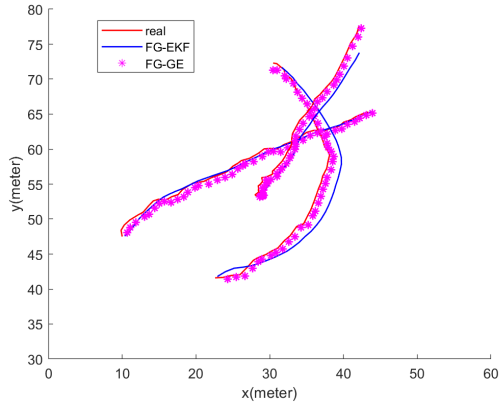

(a) Proposed joint DOA and TOA tracking algorithm

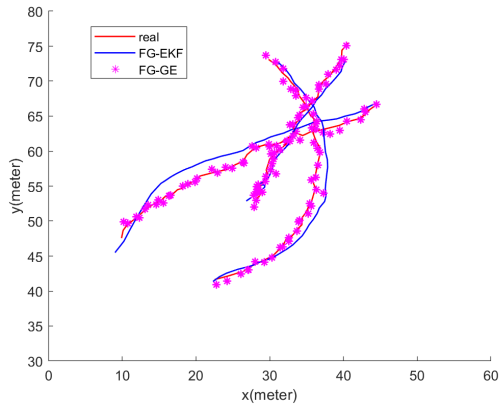

(b) DOA only based tracking algorithm

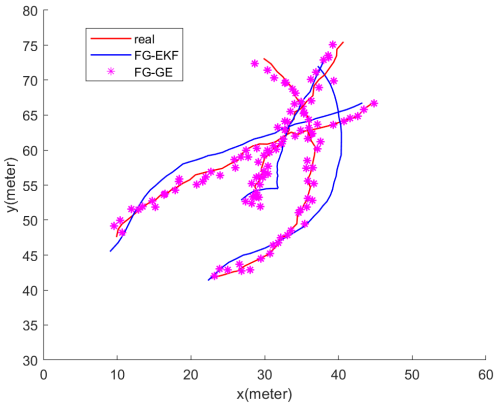

(c) TOA only based tracking algorithm

Figure 4.2: Performance comparison between the proposed and each single schemes

Table 4.1: Average RMSE comparison between the proposed and each single schemes

Average RMSE (meter)			
	Prop.FG-GE	DOA based FG-GE	TOA based FG-GE
target1	0.28	0.87	1.15
target2	0.35	0.86	1.04
target3	0.29	0.88	1.40
	Tracking with Prop.FG-GE	Tracking with DOA based FG-GE	Tracking with TOA based FG-GE
target1	0.79	1.89	2.46
target2	1.73	1.99	5.02
target3	1.92	1.89	3.35

sensors obtain 60 DOA and TOA samples having standard deviation $\sigma_\varphi = 3°$ and $\sigma_d = 15$ (meter), respectively. Let the maximum iteration time $J = 10$ and $\sigma_\omega^2 = 0.05$.

In the simulation, the proposed algorithm which performs the joint DOA-TOA algorithm, was compared with the algorithm using DOA-only and TOA-only in FG-GE and FG-GE-EKF. The estimated positions of the three targets using FG-GE, as well as the tracking trajectories using FG-GE-EKF are shown in Fig.4.2. Clearly, it can be observed that the proposed joint DOA-TOA algorithm can achieve the highest accuracy in tracking and target acquisition. The co-located targets can also be estimated based on the each previous state from proposed FG-GE-EKF. From the simulation, even though two targets intersect at a point, next state can be accurately estimated, by referring to the previous state. Moreover, to evaluate the accuracy of FG-GE and FG-GE-EKF, the average RMSE with the three algorithms was calculated, of which results are shown in TABLE 4.1.

4.3.5 Simulation Results in 3D scenario

In the 3D tracking scenario, the process equations of three targets in the $X-Y$ coordinate are the same as equations 4.14 - 4.19, and only the process equations in the Z coordinate provides additional information. The process equations in the Z coordinate used in the simulation are shown below:

$$z_{1,k} = z_{1,k-1} + \sin\left(\frac{z_{1,k-1}\Phi}{k}\right) + \omega_{z,k}, \tag{4.20}$$

$$z_{2,k} = z_{2,k-1} + \cos\left(0.2k\Phi\right) + \omega_{z,k}, \tag{4.21}$$

$$z_{3,k} = z_{3,k-1} + \left(0.03k - 0.032\right) + \omega_{z,k}. \tag{4.22}$$

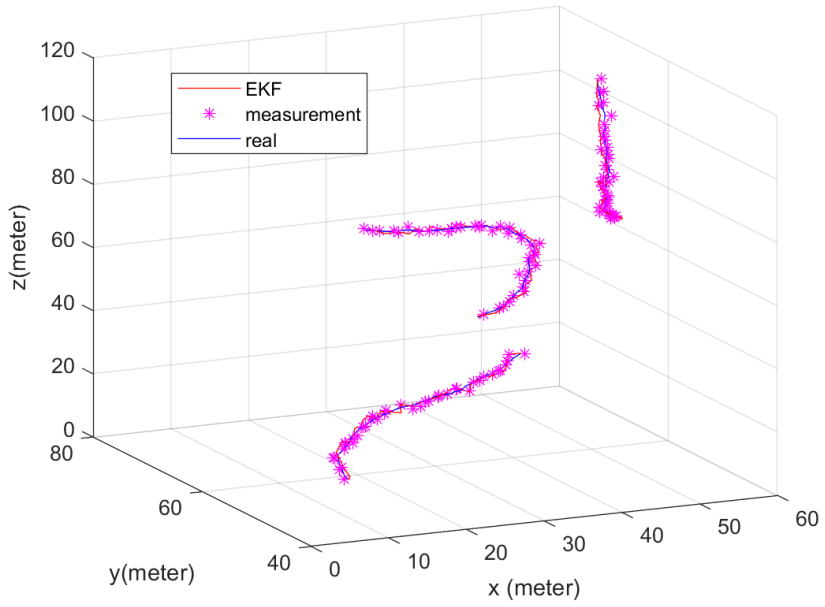

Figure 4.3: tracking trajectories in 3D scenario

All other parameters are the same as the 3D's geolocation case. By applying the proposed 3D FG-GE and FG-GE-EKF algorithms, the estimated positions of the three targets and the tracking trajectories are shown in Fig. 4.3. It is clearly seen that the estimated positions and tracking trajectories are very close to the real paths in the 3D coordinate.

Then, to evaluate the performance of the position detection and tracking of three targets, the RMSEs of 3D FG-GE and FG-GE-EKF versus timing index are calculated. The results are shown in Fig. 4.4. From the simulation results, the average RMSEs with 3D FG-GE and FG-GE-EKF are very small, which demonstrates excellent performance of the proposed algorithms.

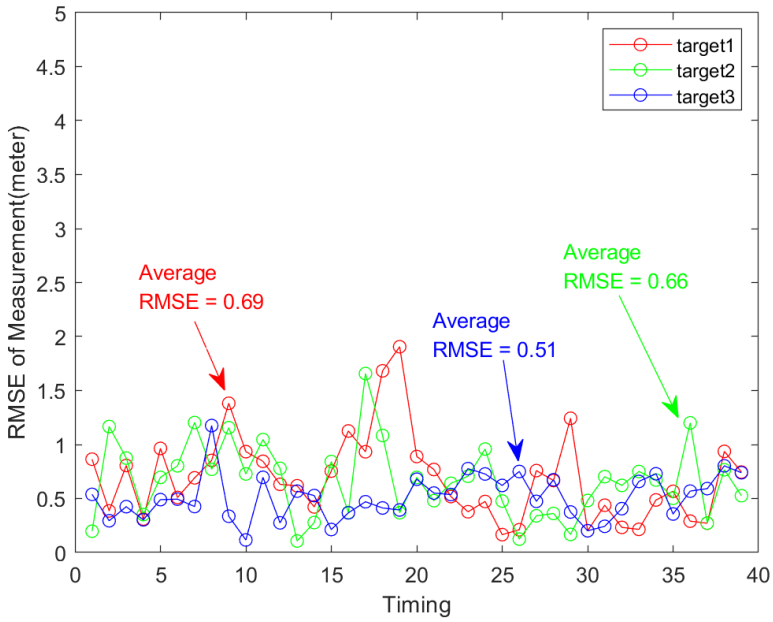

(a) The RMSE 0f 3D FG-GE

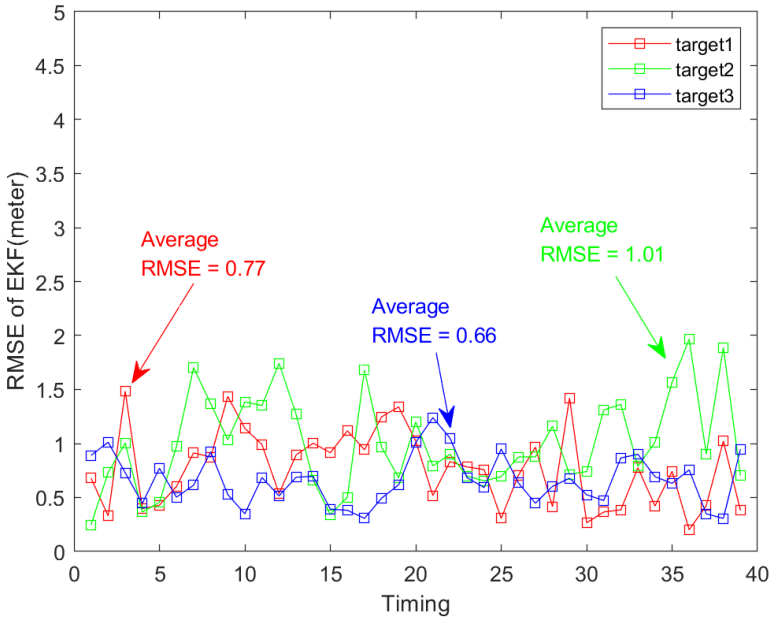

(b) The RMSE 0f 3D FG-GE-EKF

Figure 4.4: Performance of position detection and tracking in 3D scenario

Chapter 5

Information Theoretic Background

In this chapter, we provide the information theoretic background of geolocation, from the viewpoint of the relationship between Chief Executive Office (CEO) and distributed hypothesis testing (DHT) problems.

5.1 CEO and DHT problem

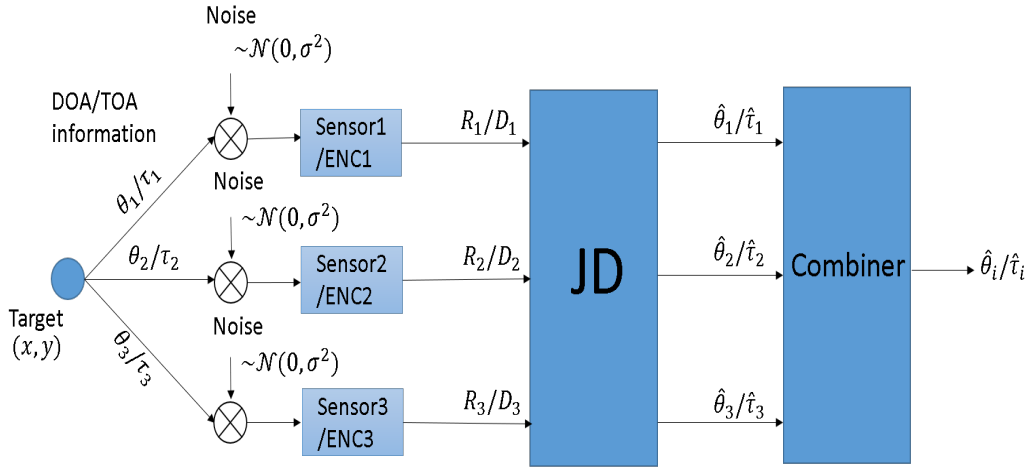

Figure 5.1: CEO problem based on Geolocation

Recently, the relationship between the CEO and DHT problems has attracted attention in the network information theory community [36, 37]. Therefore, in this chapter, we briefly describe the information theoretic background of geolocation from the viewpoint of the relationship between them. The fundamental difference between the CEO and DHT problems are:

- CEO problem discusses the rate-distortion pair of each link between the sensors and the destination, where the observations are noise corrupted,

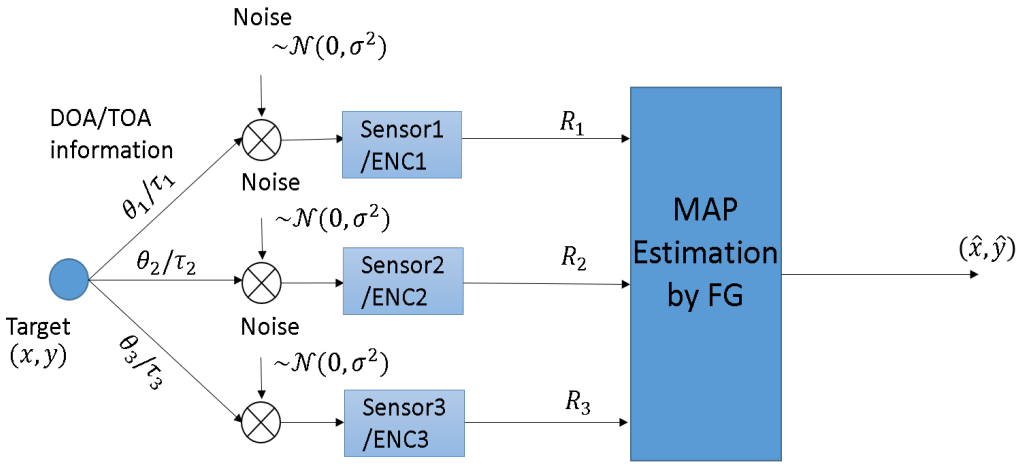

Figure 5.2: DHT based on Geolocation

and furthermore, distorted by the encoding and decoding processes. The purpose of the use of lossy encoding and decoding is because the links between sensors and the destination is not broad enough. The destination then combines the information obtained by the joint decoder (JD) to achieve the best-estimates of the observation target.

- DHT problem aims to estimate the parameters of the distribution of the sensing target, for example, mean and variance of the sensing target positions from the observations, reported to the destination. The rates of each link between the sensors and the destination are, in the same way as in the CEO problem, limited. Hence, lossy encoding and decoding are needed, however, rate-distortion pair is out of the scope for the DHT problem.

As shown in Fig. 5.1, geolocation can be seen as an example of the CEO problem, if its objective is to estimate the DOA $\hat{\theta}_i$ and TOA $\hat{\tau}_i$ of the i-th sensor, with the help of the reported DOA and TOA information from other sensors. The target position (x, y) is not the objective in this case.

On the contrary, as shown in Fig. 5.2, if the objective is to estimate the target position (x, y) from the noise-corrupted reported information of the wireless parameters, DOA and TOA, sent from all the sensors. The judgement at the center belongs to the DHT problem. The hypothesis is:

$$H_0 : (x, y) = (\hat{x}, \hat{y}) \tag{5.1}$$

$$H_1 : (x, y) \neq (\hat{x}, \hat{y}) \tag{5.2}$$

The type I error is defined by

$$Error\ type\ I : H_0\ is\ correct\ but\ H_1\ was\ chosen; \tag{5.3}$$

and the type II error is defined by

$$Error\ type\ II : H_0\ is\ incorrect\ but\ H_0\ was\ chosen. \tag{5.4}$$

In this case, the objective is to minimize type II error η_0 under the constraint that the probability of type I error is smaller than or equal to ε_0, i.e.,

$$Minimize\ Prob(typeII),$$

$$subject\ to\ Prob(typeI) \leqslant \varepsilon_0.$$

If the variance of the location (x, y) is not known, we set the acceptable deviation ε of the estimation, as

$$\sqrt{(x - \hat{x})^2 + (y - \hat{y})^2} \leqslant \varepsilon. \tag{5.5}$$

Currently, deriving the error exponent of type II, or identifying the two-dimensional curve showing the relationship between ε_0 and η_0 is a hot topic in this research area. However, more detailed analysis is out of the scope of this thesis.

Chapter 6

Conclusion and Future Work

6.1 Conclusion

In this thesis, we have proposed a distributed sensors-based wireless geolocation technique for identifying the multiple targets positions and tracking. The objective of this research is to provide a technique which can accurately estimate and track the positions of multiple targets dynamically without requiring high computation effort. Therefore, we proposed a multi-target joint TOA-DOA based geolocation and tracking algorithm both in 2D and 3D scenarios. We also proposed a new sensor association algorithm that makes correct matching between the observations and their corresponding FGs. With the proposed sensor association algorithm, the matching problem between the observations and the targets can be solved in both 2D and 3D scenarios. Furthermore, we proposed a TOA-DOA switching algorithm to compensate each technique's shortcomings. According to the simulation results, the proposed joint TOA-DOA algorithm can achieve lower average RMSEs than that with DOA-only and TOA-only techniques. The accuracy of the estimated positions of the multiple targets is evaluated by a series of simulations. The performances of the proposed FG-GE technique have been compared with the CRLB. It has been shown that the gaps between the RMSE obtained by the simulation results and the CRLB are very small even though the initial guess points are very far away from the real target positions. For the purpose of target tracking, FG of EKF is further combined with FG-GE, referred to as FG-GE-EKF, which can track multi-target dynamically both in 2D and 3D scenarios. It has been shown that the FG-GE-EKF algorithm can improve the tracking accuracy while reducing computational complexity. Finally, we have briefly discussed the relationship between the CEO and DHT problems with the scope of their application to geolocation as a theoretical basis.

6.2 Future Work

To apply the major results of this thesis to more general and practical wireless communications network-based geolocation, there are several issues left as future work, which are listed as follows:

- The major problem of TOA technique is that it requires a time reference, common to all unknown radio wave emitters, that specifies the absolute departure time of the signal transmission. Therefore, the use of TDOA instead of TOA, and combining it with DOA is reasonable to eliminate the necessity of the time reference, with the aim of the system applicability to asynchronous systems.
- In this thesis, we have only focused on estimating and tracking the target positions with one single fusion center. Since 5G, B5G and 6G systems, positioning-based services are supposed to be widely used, we should consider the combined use of the geolocation and tracking techniques from more practical viewpoint towards position-based services concept creation in wireless communication systems.
- By applying geolocation techniques in the wireless communications networks, instead of single fusion center, multiple fusion centers may be available in 5G, B5G and 6G systems where messages are exchanged, with the aim of improving the accuracy of geolocation and tracking in various practical scenarios. The common thread can be summarized as:

  (1) cooperating with other fusion centers by using backhaul networks;

  (2) achieving high gain beam forming steered stably to the users to compensate the propagation loss in high frequency bands;

  (3) utilizing the sensor diversity for the cooperation among multi-base stations;

  (4) avoiding vehicle-to-vehicle or vehicle-to-human collisions by using EKF predictor through wireless communications networks.

Appendix A

Calculation of the observation noise

In this chapter, the observation noise σ_e^2 is derived for the proposed FG-GE-EKF based on the CRLB derivation. In 2D scenario, σ_e^2 value can be derived from the measured DOA variable φ. Moreover, in 3D scenario, based on the proposed 3D FG-GE algorithm, the target position is projected onto the three planes. The observation noise of each projection point can be similarly derived from the angle information υ and γ. Due to the space limitation, only the derivation of σ_e^2 on $X-Y$ plane is provided. According to [2, 38], the CRLB is given by

$$CRLB = trace[F^{-1}(s)], \tag{A.1}$$

where F is the Fisher information matrix (FIM). Given the PDF of the variable φ with L samples, the FIM can be derived by

$$F(s) = E\left[\left(\frac{\partial}{\partial s}\ln p(\widehat{\varphi})\right)^2\right], \tag{A.2}$$

where the PDF function $p(\cdot)$ is given by

$$p(\widehat{\varphi}) = \prod_{l=1}^{L}\frac{1}{\sqrt{2\pi\sigma_\varphi^2}}\exp\left[-\frac{1}{2\sigma_\varphi^2}(\widehat{\varphi}_l-\varphi)^2\right]. \tag{A.3}$$

Moreover, (77) can be expressed by

$$E\left[\left(\frac{\partial}{\partial s}\ln p(\widehat{\varphi})\right)^2\right] = -E\left[\frac{\partial^2}{\partial\varphi^2}\ln p(\widehat{\varphi})\right]. \tag{A.4}$$

According to [35],

$$\frac{\partial^2}{\partial\varphi^2}\ln p(\widehat{\varphi}) = -\frac{L}{\sigma_\varphi^2}. \tag{A.5}$$

Then, the FIM can further be derived by

$$\begin{aligned} F(s) &= \frac{\partial \varphi}{\partial s}^T E\left[\left(\frac{\partial}{\partial \varphi}\ln p(\widehat{\varphi})\right)^T \left(\frac{\partial}{\partial \varphi}\ln p(\widehat{\varphi})\right)\right]\frac{\partial \varphi}{\partial s} \\ &= \frac{\partial \varphi}{\partial s}^T E\left[\left(\frac{\partial}{\partial \varphi}\ln p(\widehat{\varphi})\right)^2\right]\frac{\partial \varphi}{\partial s} \\ &= \frac{\partial \varphi}{\partial s}^T \left[\frac{L}{\sigma_\varphi^2}\right]\frac{\partial \varphi}{\partial s}. \end{aligned} \tag{A.6}$$

$\frac{\partial \varphi}{\partial s}$ denotes the Jacobin matrix, which is given by

$$J = \frac{\partial \varphi}{\partial s} = \begin{bmatrix} \frac{\partial \varphi_1}{\partial x} & \frac{\partial \varphi_1}{\partial y} \\ \frac{\partial \varphi_2}{\partial x} & \frac{\partial \varphi_2}{\partial y} \\ \vdots & \vdots \\ \frac{\partial \varphi_N}{\partial x} & \frac{\partial \varphi_N}{\partial y} \end{bmatrix}, \tag{A.7}$$

with

$$\frac{\partial \varphi_n}{\partial x} = \frac{Y_n - y}{d_n^2}, \tag{A.8}$$

$$\frac{\partial \varphi_n}{\partial y} = \frac{-(X_n - x)}{d_n^2}, \tag{A.9}$$

where d_n denotes the Euclidean distance between target and sensor n in $X - Y$ plane and $n = \{1, 2, \cdots, N\}$. In this paper, the prediction state $x_{k|k-1}$ and $y_{k|k-1}$ is used at timing k because the real position target (x_k, y_k) is unknown to the system. Therefore, the Jacobin matrix can be expressed by

$$J_{k|k-1} = \begin{bmatrix} \frac{Y_1 - y_{k|k-1}}{d_1^2} & \frac{-(X_1 - x_{k|k-1})}{d_1^2} \\ \frac{Y_2 - y_{k|k-1}}{d_2^2} & \frac{-(X_2 - x_{k|k-1})}{d_2^2} \\ \vdots & \vdots \\ \frac{Y_N - y_{k|k-1}}{d_N^2} & \frac{-(X_N - x_{k|k-1})}{d_N^2} \end{bmatrix}. \tag{A.10}$$

Finally, the CRLB is derived by

$$CRLB = \{\mathrm{diag}[(\mathrm{J}_{\mathrm{k|k-1}}^{\mathrm{T}} \sum\nolimits_{\varphi}^{-1} \mathrm{J}_{\mathrm{k|k-1}})\mathrm{L}]\}^{-1}. \tag{A.11}$$

References

[1] F. R. Kschischang, B. J. Frey, and H.-A. Loeliger, "Factor graphs and the sum-product algorithm," *IEEE Transactions on information theory*, vol. 47, no. 2, pp. 498–519, 2001.

[2] H. Wymeersch, *Iterative receiver design*. Cambridge University Press Cambridge, 2007, vol. 234.

[3] M. R. K. Aziz, K. Anwar, and T. Matsumoto, "Factor graph-based geolocation techniques for position detection of unknown radio wave emitter," Ph.D. dissertation, School of Information Science, Japan Advanced Institute of Science and Technology, Japan, 2016.

[4] J. J. Caffery and G. L. Stuber, "Overview of radiolocation in cdma cellular systems," *IEEE Communications Magazine*, vol. 36, no. 4, pp. 38–45, 1998.

[5] S. A. A. Shah, E. Ahmed, M. Imran, and S. Zeadally, "5g for vehicular communications," *IEEE Communications Magazine*, vol. 56, no. 1, pp. 111–117, 2018.

[6] I. Aydin, M. Karakose, and E. Karakose, "A navigation and reservation based smart parking platform using genetic optimization for smart cities," in *2017 5th International Istanbul Smart Grid and Cities Congress and Fair (ICSG)*. IEEE, 2017, pp. 120–124.

[7] R. Mautz, "Indoor positioning technologies," 2012.

[8] D. Tandur, M. Gandhi, H. Kour, and R. Gore, "An iot infrastructure solution for factories," in *2017 22nd IEEE International Conference on Emerging Technologies and Factory Automation (ETFA)*. IEEE, 2017, pp. 1–4.

[9] P. Inghelbrecht, "System and method for tracking vehicle operation through user-generated driving incident reports," Dec. 29 2011, uS Patent App. 13/168,786.

[10] H. Wymeersch, G. Seco-Granados, G. Destino, D. Dardari, and F. Tufvesson, "5g mmwave positioning for vehicular networks," *IEEE Wireless Communications*, vol. 24, no. 6, pp. 80–86, 2017.

[11] K. E. Skouby and P. Lynggaard, "Smart home and smart city solutions enabled by 5g, iot, aai and cot services," in *2014 International Conference on Contemporary Computing and Informatics (IC3I)*. IEEE, 2014, pp. 874–878.

[12] P. Lynggaard and K. E. Skouby, "Deploying 5g-technologies in smart city and smart home wireless sensor networks with interferences," *Wireless Personal Communications*, vol. 81, no. 4, pp. 1399–1413, 2015.

[13] J. C. Chen, K. Yao, and R. E. Hudson, "Source localization and beamforming," *IEEE Signal Processing Magazine*, vol. 19, no. 2, pp. 30–39, 2002.

[14] B. E. Caroline, S. C. Xavier, A. P. Kabilan, and J. William, "Performance analysis and comparison of optical signal processing beamforming networks: a survey," *Photonic Network Communications*, vol. 37, no. 1, pp. 38–52, 2019.

[15] F. Liu, P. Zhao, and Z. Wang, "Ekf-based beam tracking for mmwave mimo systems," *IEEE Communications Letters*, vol. 23, no. 12, pp. 2390–2393, 2019.

[16] P. Papadimitratos and A. Jovanovic, "Gnss-based positioning: Attacks and countermeasures," in *MILCOM 2008-2008 IEEE Military Communications Conference*. IEEE, 2008, pp. 1–7.

[17] J.-C. Chen, Y.-C. Wang, C.-S. Maa, and J.-T. Chen, "Network-side mobile position location using factor graphs," *IEEE Transactions on Wireless Communications*, vol. 5, no. 10, pp. 2696–2704, 2006.

[18] W. H. Foy, "Position-location solutions by taylor-series estimation," *IEEE Transactions on Aerospace and Electronic Systems*, no. 2, pp. 187–194, 1976.

[19] Y. Kanayama, Y. Kimura, F. Miyazaki, and T. Noguchi, "A stable tracking control method for an autonomous mobile robot," in *Proceedings., IEEE International Conference on Robotics and Automation*. IEEE, 1990, pp. 384–389.

[20] T. Drescher, W. Kreuzer, and J. Nielson, "Rocket trajectory correction using strap-on gps guided thrusters," in *IEEE 1998 Position Location and Navigation Symposium (Cat. No. 98CH36153)*. IEEE, 1996, pp. 387–394.

[21] T. ÇImen and S. P. Banks, "Nonlinear optimal tracking control with application to super-tankers for autopilot design," *Automatica*, vol. 40, no. 11, pp. 1845–1863, 2004.

[22] Z. Cai and L. Feng, "Eyeball tracking method and apparatus, and device," Jun. 30 2020, uS Patent 10,699,420.

[23] R. Mautz, "Overview of current indoor positioning systems," *Geodezija ir kartografija*, vol. 35, no. 1, pp. 18–22, 2009.

[24] F. Adib, Z. Kabelac, and D. Katabi, "Multi-person localization via {RF} body reflections," in *12th {USENIX} Symposium on Networked Systems Design and Implementation ({NSDI} 15)*, 2015, pp. 279–292.

[25] T. F. Sanam and H. Godrich, "Comute: A convolutional neural network based device free multiple target localization using csi," *arXiv preprint arXiv:2003.05734*, 2020.

[26] J.-C. Chen, P. Ting, C.-S. Maa, and J.-T. Chen, "Wireless geolocation with toa/aoa measurements using factor graph and sum-product algorithm," in *IEEE 60th Vehicular Technology Conference, 2004. VTC2004-Fall. 2004*, vol. 5. IEEE, 2004, pp. 3526–3529.

[27] H.-L. Jhi, J.-C. Chen, C.-H. Lin, and C.-T. Huang, "A factor-graph-based toa location estimator," *IEEE transactions on wireless communications*, vol. 11, no. 5, pp. 1764–1773, 2012.

[28] C. Mensing and S. Plass, "Tdoa positioning based on factor graphs," in *2006 IEEE 17th International Symposium on Personal, Indoor and Mobile Radio Communications*. IEEE, 2006, pp. 1–5.

[29] C.-T. Huang, C.-H. Wu, Y.-N. Lee, and J.-T. Chen, "A novel indoor rss-based position location algorithm using factor graphs," *IEEE Transactions on Wireless Communications*, vol. 8, no. 6, pp. 3050–3058, 2009.

[30] S. N. Karimah, M. R. K. Aziz, and T. Matsumoto, "A hybrid toa and rss-based factor graph for wireless geolocation technique," in *2016 IEEE 12th International Colloquium on Signal Processing & Its Applications (CSPA)*. IEEE, 2016, pp. 140–145.

[31] S. Baker and I. Matthews, "Lucas-kanade 20 years on: A unifying framework," *International journal of computer vision*, vol. 56, no. 3, pp. 221–255, 2004.

[32] Y. Chan, A. Hu, and J. Plant, "A kalman filter based tracking scheme with input estimation," *IEEE transactions on Aerospace and Electronic Systems*, no. 2, pp. 237–244, 1979.

[33] N. Wang and D.-Y. Yeung, "Learning a deep compact image representation for visual tracking," *Advances in neural information processing systems*, vol. 26, pp. 809–817, 2013.

[34] M. Cheng, M. R. K. Aziz, and T. Matsumoto, "A doa-based factor graph technique for 3d multi-target geolocation," *IEEE Access*, vol. 7, pp. 94 630–94 641, 2019.

[35] ——, "Integrated factor graph algorithm for doa-based geolocation and tracking," *IEEE Access*, vol. 8, pp. 49 989–49 998, 2020.

[36] Y. Ugur, I. E. Aguerri, and A. Zaidi, "Vector gaussian ceo problem under logarithmic loss," in *2018 IEEE Information Theory Workshop (ITW)*. IEEE, 2018, pp. 1–5.

[37] R. Olfati-Saber, E. Franco, E. Frazzoli, and J. S. Shamma, "Belief consensus and distributed hypothesis testing in sensor networks," in *Networked Embedded Sensing and Control*. Springer, 2006, pp. 169–182.

[38] M. R. K. Aziz, K. Anwar, and T. Matsumoto, "A new doa-based factor graph geolocation technique for detection of unknown radio wave emitter position using the first-order taylor series approximation," *EURASIP Journal on Wireless Communications and Networking*, vol. 2016, no. 1, p. 189, 2016.

Achievements

[1] L. Jiang, M. Cheng and T. Matsumoto, "A TOA-DOA Hybrid Factor Graph-based Technique for Multi-Target Geolocation and Tracking" *IEEE Access*, vol. 9, pp. 14203-14215, Jan, 2021.

[2] L. Jiang, M. Cheng and T. Matsumoto, "Research on arrival direction estimation, position estimation technology, etc," *Project report to Hitachi Kokusai Electric Inc.*, Jan. 2021.